STRESS ANALYSIS USING DEFORMATION LAMELLAE IN QUARTZ

STRESS ANALYSIS USING DEFORMATION LAMELLAE IN QUARTZ

By

Kathryn M. Bethune

A Thesis

Submitted to the Faculty of Science

in Partial Fulfillment of the Requirements

for the Degree

Bachelor of Science

McMaster University

April, 1986

Honours Bachelor of Science, 1986 (Geology)

McMaster University
Hamilton, Ontario

TITLE: Stress Analysis using deformation lamellae in quartz

AUTHOR: Kathryn M. Bethune

SUPERVISOR: Dr. P.M. Clifford

NUMBER OF PAGES: viii, 84 p.

To Mom and Dad, Wendy and Rick, Brian and Eva, Cheri and Bob, Leslie and Dave and to all those special teachers past and present. This is for you.

ABSTRACT

Orientations of deformation lamellae in quartz and C-axes of quartz grains containing lamellae were measured at seven locations across a gently folded bed of the Oriskany Sandstone, central Pennsylvania. Lamellae so measured have an average inclination of 20^{o}-30^{o} to the basal plane, and are therefore categorized as "subbasal".

Fabrics of poles to deformation lamellae and corresponding C-axis orientations suggest a paleostress field for the fold which had the arrangement; σ_1 bedding parallel, σ_3 bedding perpendicular, and σ_2 fold axis subparallel. Relative magnitudes of the stresses were given by the condition $\sigma_1 > \sigma_3$. σ_2 is believed to have varied in magnitude between σ_1 and σ_3 during fold development.

Exact timing of formation of lamellae is uncertain. Textural evidence shows that they predate a later generation of compressional and tensional microfractures associated with the deformation. The best explanation is that they formed in early stages of layer parallel compaction when compressive stresses in all zones of the fold were greatest. Stress refraction may or may not have been operative.

ACKNOWLEDGEMENTS

Many thanks to all who played integral roles in the production of this thesis: to Paul Clifford and Dave Collins, for suggesting a topic and helping me get started; to Frank Fueten, who gave much of his time and effort to help me process the data; to Adrian Roggeband and Pam Collins, who assissted with the drafting and typing; and finally to Jack Whorwood and Len Zwicker for their technical help. Thankyou once more. It would have been impossible without all of you.

An extra special thanks goes to my supervisor and good friend, P.M.C. . Your terrific amount of support, as well as your all-round positive thinking are much appreciated. I have learned a lot!

TABLE OF CONTENTS

LIST OF FIGURES

CHAPTER 1

1.1 Definition

By deformation lamellae, we refer to the closely-spaced, approximately planar, sub-parallel zones which pervade many of the quartz grains in the sandstone under study. Such structures were first described by Bohm (1883).

Typically the lamellae are decorated with reddish-brown, granular inclusions; they are also often wavy, rather than planar, and are found most commonly at high angles or perpendicular to zones of undulatory extinction. In the past, lamellae have been recognized in two distinct habits: in one they are confined to individual grains; in another, they show a remarkable persistance in orientation over an area of several grains.

In this study, lamellae of both types have been observed. Some tend to pervade entire grains, without penetrating interstitial cement (see Fig. 1). Others persist in orientation through several grains, as well as through intervening cement (see Fig. 2). Of these, the former are the more common. This suggests the lamellae were formed prior to, or just at the onset of, crystallization of the secondary quartz cement.

1.2 Introduction

Deformation of quartz at relatively low strain produces three types of microstructures: undulatory extinction, deformation bands, and deformation lamellae.

Fig. 1 Photomicrographs showing deformation lamellae which are confined within quartz grains.

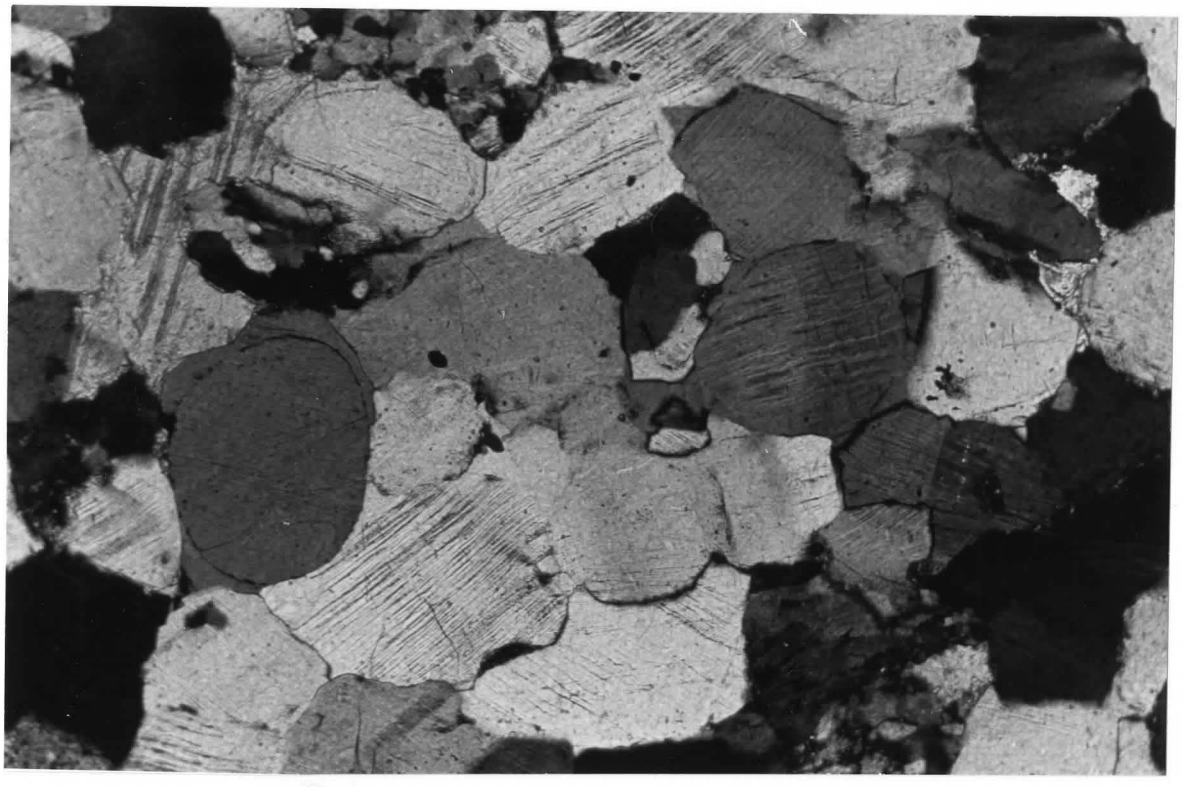

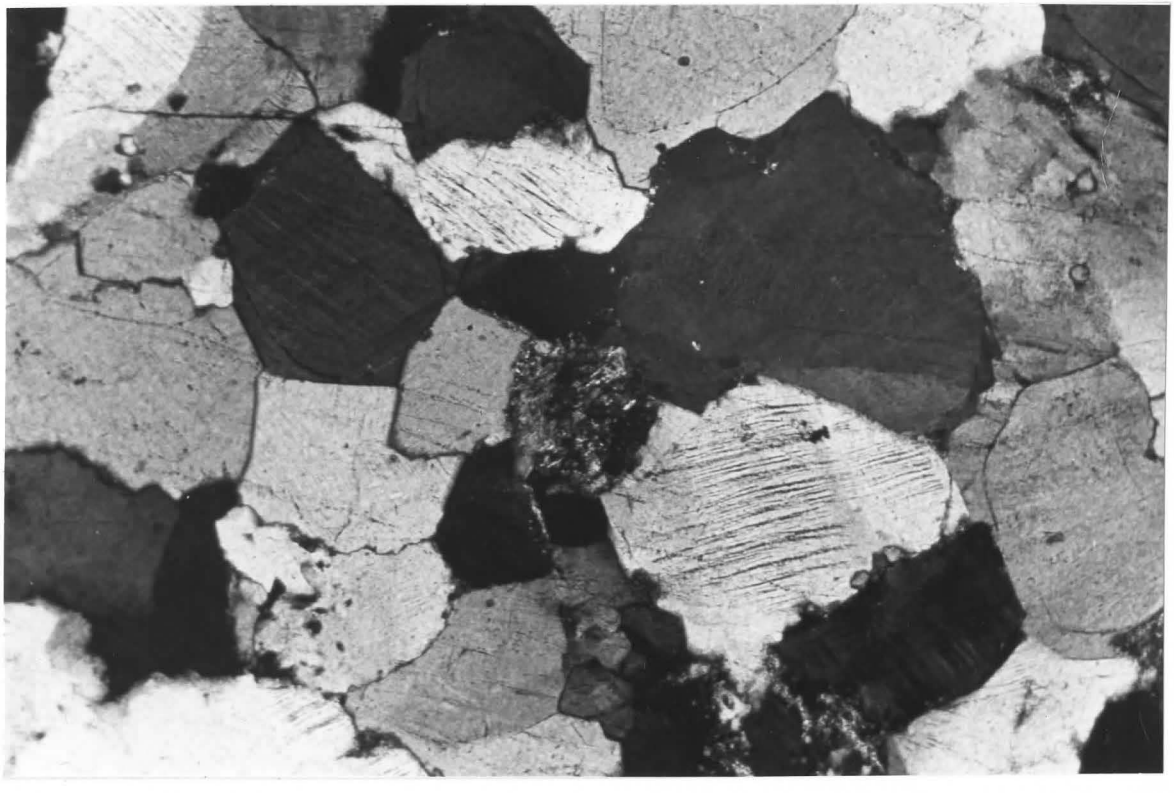

Fig. 2 Photomicrograph of deformation lamellae which persist in orientation through several grains, as well as through intervening cement.

Much research has been conducted over the past two and a half decades in an effort to understand the relationship between these structures and the natural conditions of their formation. In particular, it is thought that fabrics which include deformation lamellae can act as guides to their causative stress field. This idea was first explored by Hansen and Borg (1962) in the stress analysis of a folded section of the Oriskany Sandstone. They compared the orientation of principal stresses derived from calcite twin lamellae (Turner's method, 1953) with those derived from deformation lamellae in quartz. The results from each method were in good agreement; they concluded that the fabrics of deformation lamellae could act as independent guides to the paleostress field.

At the time of Hansen and Borg's study (1958), the actual origin of deformation lamellae was still somewhat enigmatic. Christie and Raleigh (1959) postulated that lamellae were kink bands generated on planes at high angles to the C-axis (see Fig. 3). This interpretation was based on fabric analysis in naturally deformed quartzites. However, the lamellae had still not been produced experimentally. It was not until 1964 that a clearer picture began to emerge. This came via experiments of Carter, Christie and Griggs (1964). These researchers used a variety of high pressure apparatus to simulate conditions of natural deformation and succeeded in producing all three microstructures. Analysis of the fabrics of the deformation lamellae in relation to known stress fields

Fig. 3 Two dimensional sketch of the process of formation of deformation lamellae (as modified from Christie and Raleigh, 1959, p. 403).

(a) uniform parallel lines in grains x and y and short lines in other grains indicate the orientations of the C-axes; irregular lines in grains x and y represent deformation lamellae. Only grains which have suitably oriented C-axes (45^{o} to σ_1) contain deformation lamellae.

(b,c,d) Change in shape of a grain of initially circular cross section as a result of (1) shearing on surfaces parallel to (0001)=C-axis; and (2) kinking along planes at a high angle to (0001)=C-axis. The external rotation (E.R.) of the grain is shown qualitatively. The production of kink bands is a necessary consequence of the restriction on shearing imposed by other grains.

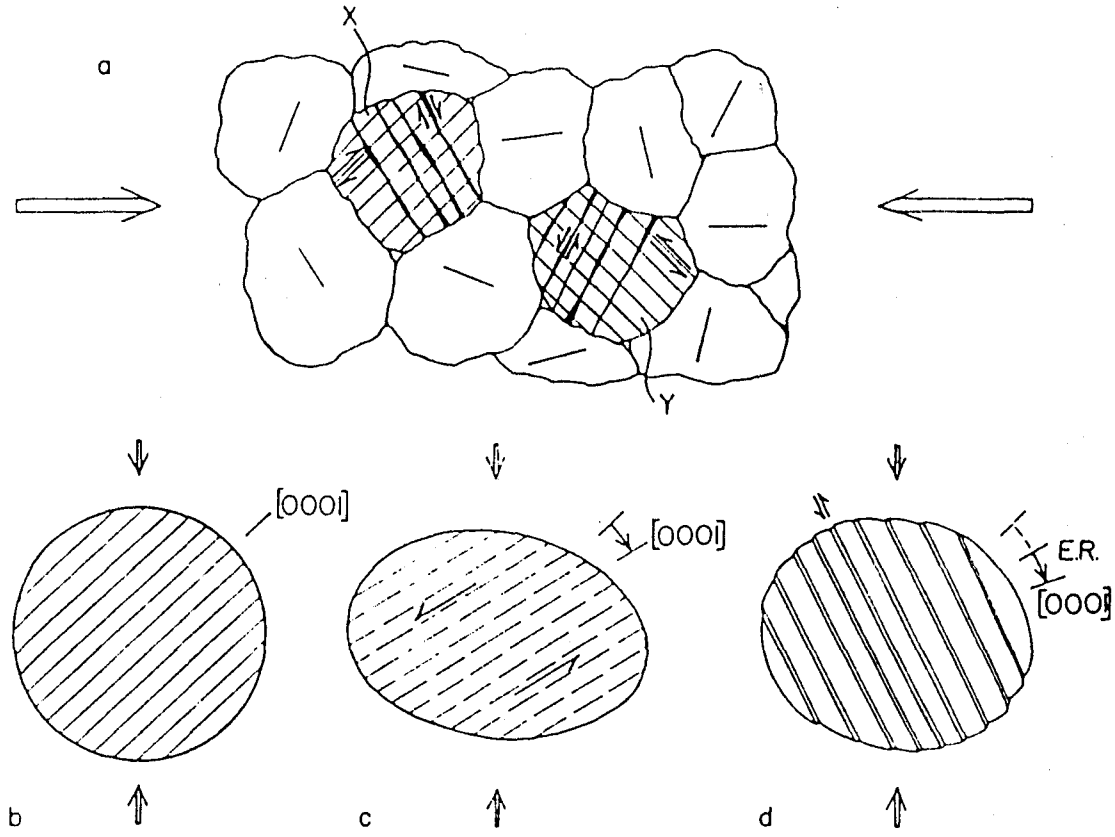
a
X
Y
[0001]
b
[0001]
c
E.R.
[0001]
d

gave a better understanding of possible geometrical relationships. For example, it was found that poles to deformation lamellae generally defined a small circle girdle of radius 30^{o}-60^{o} about the maximum principal stress. This reinforced previous opinion that the lamellae were formed on planes of maximum resolved shear stress at an average angle of 45^{o} from σ_1. It also agreed with earlier observations that poles to quartz lamellae in naturally deformed rocks had the common distribution of two point maxima 90^{o} apart (Fairbairn and Turner, 1948).

The geometric relationship between C-axis orientation and lamellae orientaion was also explored. Results indicated that experimentally formed lamellae occured in three distinct orientations. The most common was at small inclinations to the basal plane. A weaker development of lamellae was found at 20^{o}-60^{o} from the basal plane, and the sparsest population occurred sub-parallel to the C-axis.

The same general trends were observed naturally in deformed rocks. An exception was that the lamellae of natural deformations had a higher average inclination to the basal plane (10^{o}-30^{o} as opposed to 0-12^{o}). Other slip mechanisms were also thought to be operative in cases where lamellae formed despite there being low shear stress on (0001).

Extensive investigation of quartz microstructres continued following the initial work of Carter, Christie

and Griggs (1964). Experiments of Heard and Carter (1968) explored the mechanism of lamellae formation as it related to increasing temperature and decreasing strain rate (see Fig. 4). They found that at lower temperatures and higher strain rates mechanisms of basal slip and cataclasis were dominant. As temperature increased and strain rate decreased this mechanism gave way to a subbasal mechanism (10^{O}-30^{O} from base) and finally to a field in which lamellae developed in all orientations, designated as the "relatively non-selective field" (see Carter, 1976, p. 322). Lamellae orientations were also examined in relation to known stress fields. Previous observations were confirmed; that is, poles to lamellae were found in small circle girdles about the principal stress. Also relevant were the observations that lamellae were statistically inclined to σ_1 at angles lower than the basal plane, and that poles to lamellae and C-axes in relatively more or less deformed parts of individual grains were cozonal (see Fig. 5 for explanation).

In addition to variables of temperature and strain rate, Ave'Lallemant and Carter (1971) examined the relationship between mechanism and pressure (see Fig. 6). A three dimensional phase diagram was constructed so as to show the dependence of mechanism on these variables (see Fig. 7). A significant observation was that lamellae of subbasal orientation would be expected to form under most crustal conditions as is commonly observed (see Carter, 1976, p. 322).

Fig. 4 Experimental results of Heard and Carter (1968). Lamellae form via basal slip mechanisms at low temperatures and high strain rates, and via a subbasal mechanism at high temperatures and low strain rates.

QUARTZ SINGLE CRYSTALS
O^+ ORIENTATION

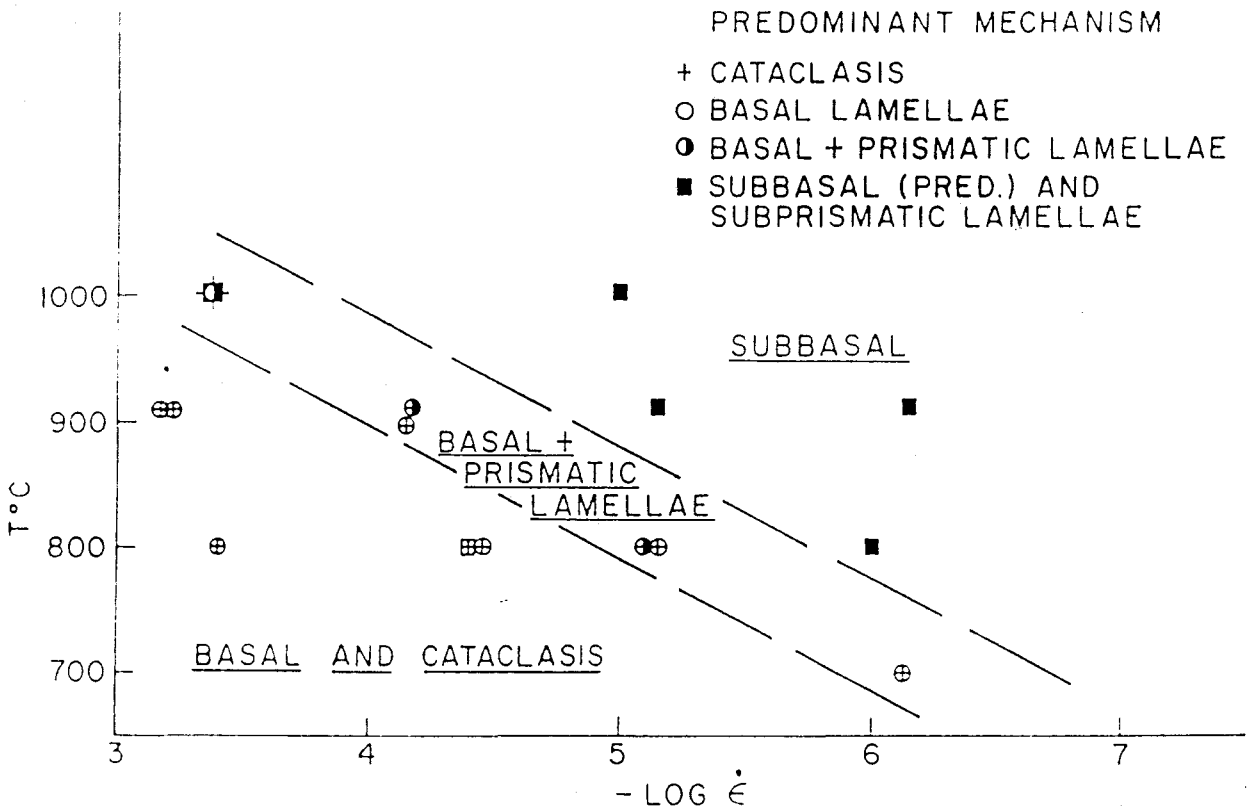

Fig. 5 (as modified from Carter, Christie and Griggs, 1964, p. 741)

(a) Sketch of a grain in an experimentally deformed quartzite showing closer spacing of lamellae (l_2) in more highly deformed regions (C_2), than in less deformed regions (C_1). C_2 has rotated toward σ_1 with respect to C_1.

(b) Diagram showing geometry of rotations indicated in (a). C_1 is inclined at higher angles to σ_1 than C_2. C_1 and C_2 are "cozonal".

(c) Great circles connect C-axes as measured above. Open circles are C_1 measurements while closed circles are C_2 measurements. In all cases C-axes in more highly deformed regions (C_2) are closer to σ_1 than those in less deformed regions (C_1).

σ_1
c.
b.
E.R.
C_2
C_1
l_2
l_1
a.

Fig. 6 Temperature versus Confining Pressure graph showing various "mechanism" fields for lamellae formation (Ave'Lallemant and Carter, 1971).

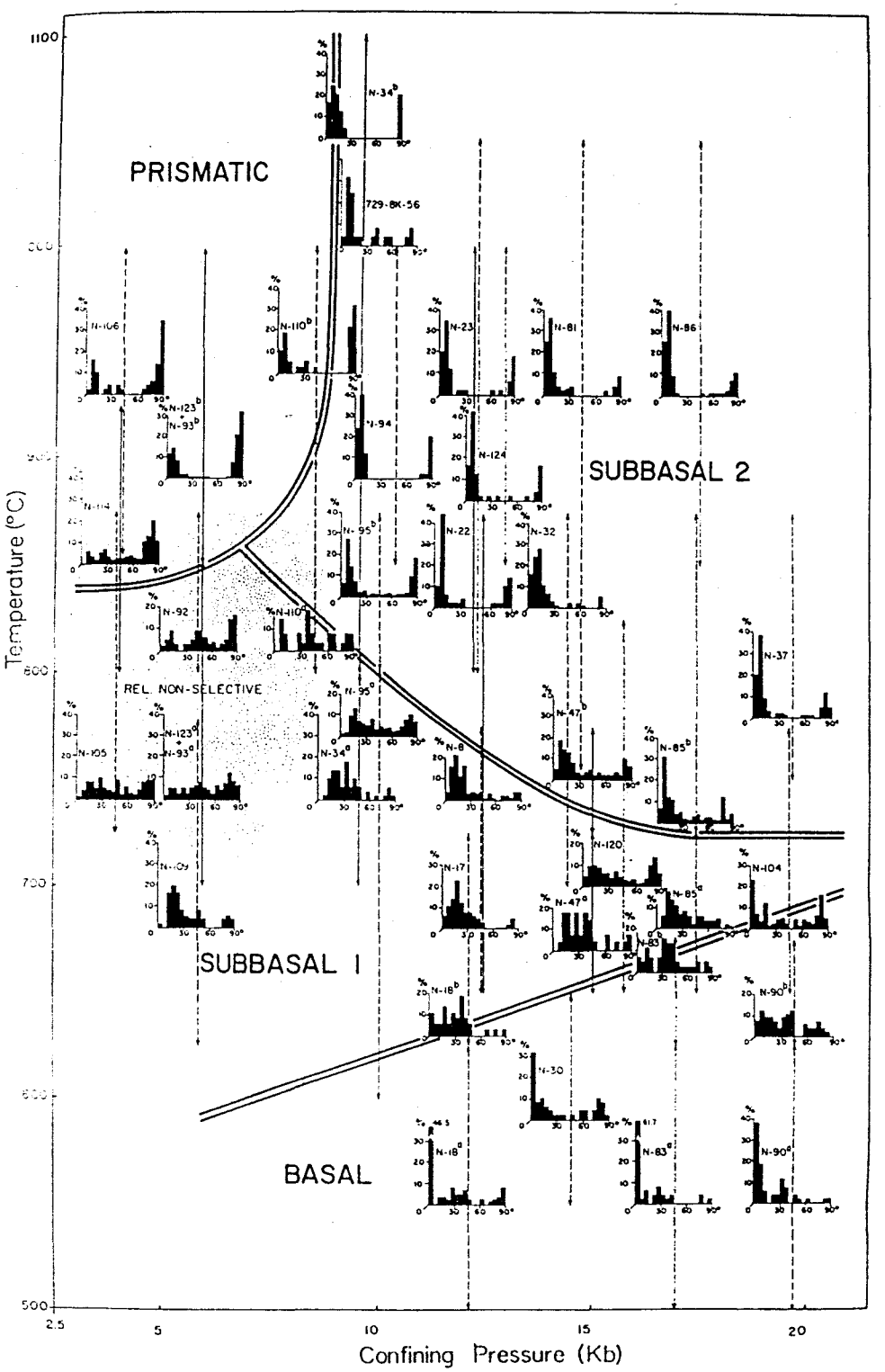
PRISMATIC
SUBBASAL 2
REL. NON-SELECTIVE
SUBBASAL I
BASAL
Temperature (°C)
Confining Pressure (Kb)
1100
900
800
700
600
500
2.5
5
10
15
20

Fig. 7 Three dimensional phase diagram (Ave'Lallemant and Carter, 1971) showing the dependence of machanism of lamellae formation on the variables of temperature, pressure, and strain rate.

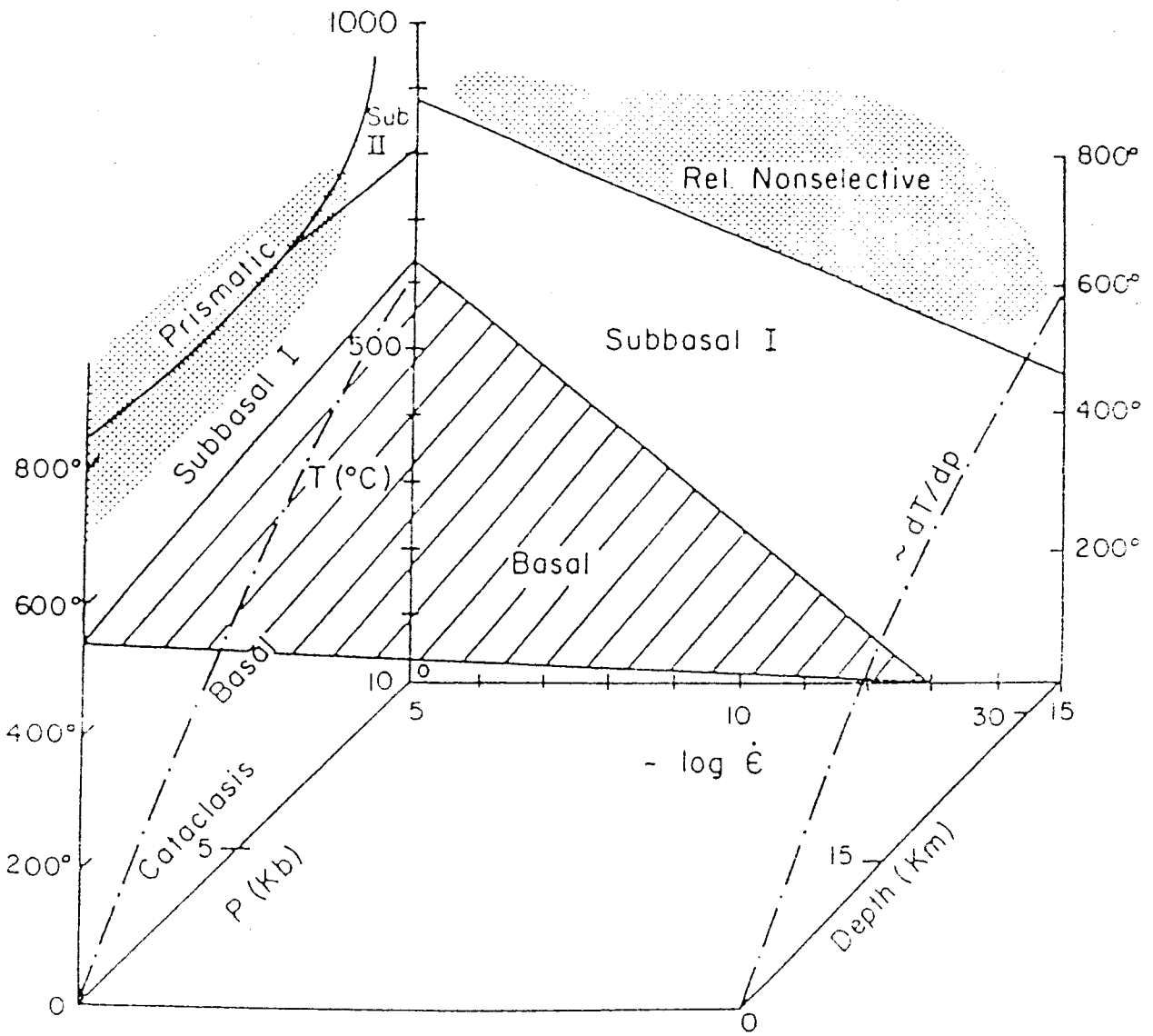
1000
Sub II
Prismatic
Rel. Nonselective
800°
600°
400°
200°
Subbasal I
500
T (°C)
Subbasal I
Basal
~ dT/dp
Basal
10
0
5
10
30
15
- log ε̇
Cataclasis
5
P (Kb)
15
Depth (Km)
0
0

1.3 More Recent Work

The SEM and TEM have been valuable tools for investigating geological microstructures since the late nineteen sixties. The development of dislocation theory throughout this time period has also had a tremendous influence on our understanding of microstructural development. Various authors have attempted to understand the mechanisms of deformation in quartz. From their investigations, several generalizations can be made concerning deformation lamellae (taken from White, 1973b).

1. Lamellae can be subdivided into 2 groups:
   (a) lamellae along rational lattice planes, normally sub-parallel to the basal plane or less frequently sub-parallel to the prism plane.
   (b) lamellae parallel to rational lattice planes with the basal plane being most common.

2. Irrational lamellae tend to form at low strain rates and high temperatures (metamorphic rocks) whereas rational lamellae occur in quartz which has been subjected to high strain rates (impactites).

3. The tendency to form lamellae increases with increasing (OH) content.

4. The above lamellae have been interpreted as any of the following defects: (i) subgrain walls; (ii) narrow subgrains; (iii) deformation twins; (iv) fractures; (v) dislocation debris in slip bands; (vi) zones of tangled dislocations (experimental rocks only); (vii) thin zones of glass (Christie and Ardell, 1974); and (viii) plane phase objects (artifacts resulting from objects smaller than resolving power of optical microscope and devoid of information about the object) (McLaren, 1970).

5. For many of these defects (i.e. i, iii, iv), decoration with voids (bubbles) or particles of a different phase (glass) is necesary before they can be imaged as phase objects and thus viewed in an optical microscope.

Due to the numerous types of features which can be viewed as deformation lamellae, one might question the viability of using them as guides to stress orientations. According to White (1973b) only lamellae of category (v) fit in with the model of slippage on the basal plane, as proposed by Carter, Christie and Griggs (1964). Fracture and deformation twins (categories (iii) and (iv)) might also be useful for stress determinations, providing internal stresses within the rock are homogeneous. However, metallurgial evidence suggests the contrary (see White, 1973b, p. 28).

Despite such misgivings, Carter (1976) emphasizes that there is more than ample empirical evidence, both from experimental and natural samples, to indicate that natural subbasal quartz lamellae are reliable indicators of paleo-stress and/or strain axes.

1.4 Application to Dynamic Systems - Stress Analysis

Three methods exist for determining principal stresses from deformation lamellae (Carter and Raleigh, 1969). The methods are applicable to lamellae inclined at roughly 10^{o}-30^{o} to (0001). They are:

(1) The acute-angle method - lamellae are inclined statistically at angles smaller than 45^{o} to σ_1 (This is viewed as the least reliable method since most of the lamellae in specimens have an average inclination of 45^{o} to σ_1).

(2) The C_0-C_1 method - planes contaning C_0 and C_1 in individual grains intersect in σ_1 (for $\sigma_1 > \sigma_2 = \sigma_3$) or σ_3 (for $\sigma_3 < \sigma_1 = \sigma_2$) or contain σ_1 and σ_3 (for $\sigma_1 > \sigma_2 > \sigma_3$), with C_1 oriented closest to σ_1 (see Fig. 5).

(3) The arrow method - arrows connect stereoplot positions of C-axes (tail) and poles to lamellae (head) of individual grains. Arrows point toward σ_3 (for $\sigma_3 < \sigma_1 = \sigma_2$), towards a great circle containing σ_2 and σ_3 (for $\sigma_1 > \sigma_2 = \sigma_3$), or contain σ_1 and σ_3 (for $\sigma_1 > \sigma_2 > \sigma_3$).

Three studies have utilized such applications in the past. All have involved analysis of a folded layer of calcareous sandstone (Hansen and Borg, 1962; Scott et al., 1965; Carter and Friedman, 1965).

Both Hansen & Borg and Carter & Friedman inferrred directions of stress using both deformation lamellae and calcite twin lamellae. Hansen and Borg used methods (1) and (3) above, while Carter and Friedman used all three methods. In both studies, results from methods involving deformation lamellae were found to be internally consistent, as well as consistent with results from calcite twinning. As mentioned earlier, this confirmed the reliability of fabrics of deformation lamellae as independent indicators of paleostress orientations. Further confirmation of this idea was given by Scott et al. (1965), who attempted a dynamic interpretation of a fold using deformation lamellae alone. Scott concluded that the deformation lamellae formed early in the history of the fold due to horizontal compression parallel to bedding, and had subsequently been passively rotated into their final position.

This contrasted with an earlier opinion (Christie and Raleigh, 1959) which viewed lamellae as having been formed in a late stage, compressive event. An explanation

for these differing interpretations can be given by considering the contrasting geologic settings of each study. Where Christie and Raleigh were examining deformation lamellae from a quartzite in an isoclinal fold, Scott et al. were looking at lamellae in a minor concentric fold of a much less deformed region. Thus, the former of these settings might have experienced "overprinting" of original lamellae fabrics due to metamorphism, whereas the latter would more likely have preserved information about original dynamics. It is also likely that the metamorphic regime favoured more complicated and varied mechanisms of lamellae formation.

The fold which is the subject of this study occurs in a geologic setting similar to that of Scott et al. (1965). For this reason it is conceivable that the same approach as Scott et al. (1965) would be applicable here; that is, the fabrics of the deformation lamellae should give some clue to the dynamic history of folding. In particular, it should be possible to state whether the lamellae were early or late with respect to the deformation process, and to get an idea of the approximate values of strain rate, temperature, and pressure necessary to produce the fold.

1.5 Nature of the Fold - Geologic Setting

The fold occurs in the Valley and Ridge Province of the Appalachian orogen, and is a broad anticline of class 1B (see Fig. 8). The north limb is cut by a small thrust

Fig. 8 Annotated sketch of folded bed (from Buhay, 1985). Stations where samples were collected are displayed.

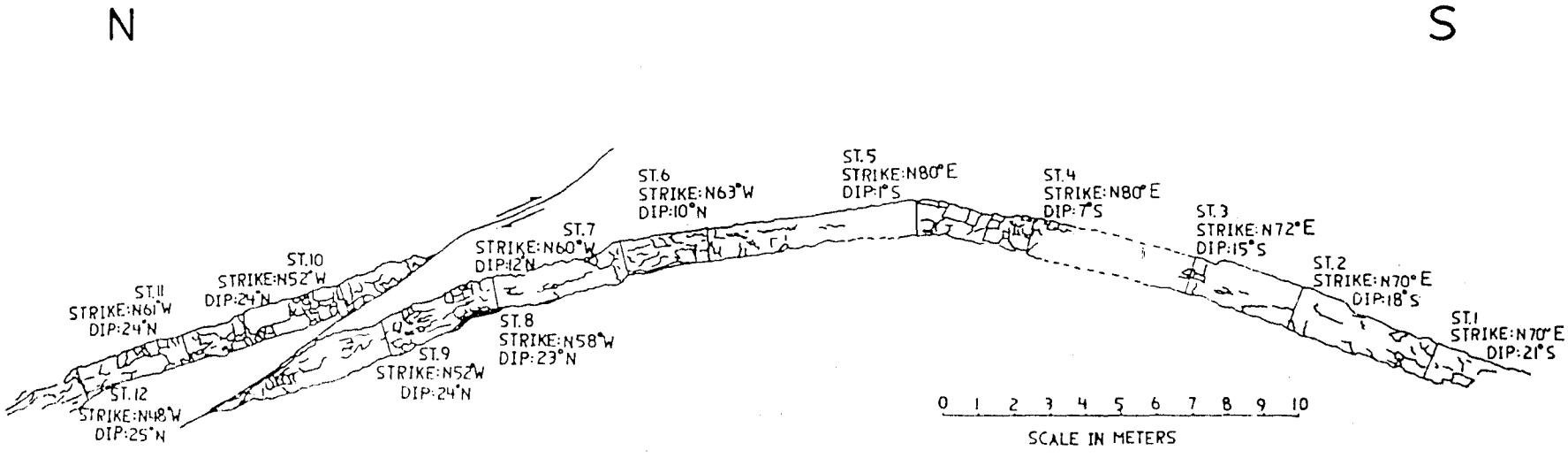
N
S
ST.1
STRIKE:N70°E
DIP:21°S
ST.2
STRIKE:N70°E
DIP:18°S
ST.3
STRIKE:N72°E
DIP:15°S
ST.4
STRIKE:N80°E
DIP:7°S
ST.5
STRIKE:N80°E
DIP:1°S
ST.6
STRIKE:N63°W
DIP:10°N
ST.7
STRIKE:N60°W
DIP:12°N
ST.8
STRIKE:N58°W
DIP:23°N
ST.9
STRIKE:N52°W
DIP:24°N
ST.10
STRIKE:N52°W
DIP:24°N
ST.11
STRIKE:N61°W
DIP:24°N
ST.12
STRIKE:N48°W
DIP:25°N
0 1 2 3 4 5 6 7 8 9 10
SCALE IN METERS

fault. Work has concentrated on an isolated bed in the fold, 1.1 m thick.

The outcrop itself is located in central Pennsylvania (see Fig. 9). Here, the formation involved in folding is the Oriskany Sandstone. This folded interval of the Oriskany was studied in a B.Sc. thesis by William Buhay (1985). Buhay attempted to propose a model for folding of a distinct, massive bed within the Oriskany based on analysis of microfractures. A preconceived notion was that such a bed would have had to bend via the mechanism of tangential longitudinal strain (Ramsay, 1967). The data Buhay collected supported this notion. In particular, he developed a classification of extentional versus compressional microfractures. Through careful mapping of the positions of these he was able to suggest a position for the neutral surface. Measurements of gapes and overlap of the fractures also enabled him to estimate the amount of strain involved. A comparison to the theoretical position of the neutral surface, as calculated from the radius of curvature of the fold, revealed that much more strain had been accomodated in folding than theory would have predicted. Buhay attributed the extra strain to have been derived from layer parallel shortening before significant bending was initiated.

The microfractures studied by Buhay clearly post-date the generation of the deformation lamellae (see Section 3.7, Fig. 21).

Fig. 9 Location map of study area (from Buhay, 1985).

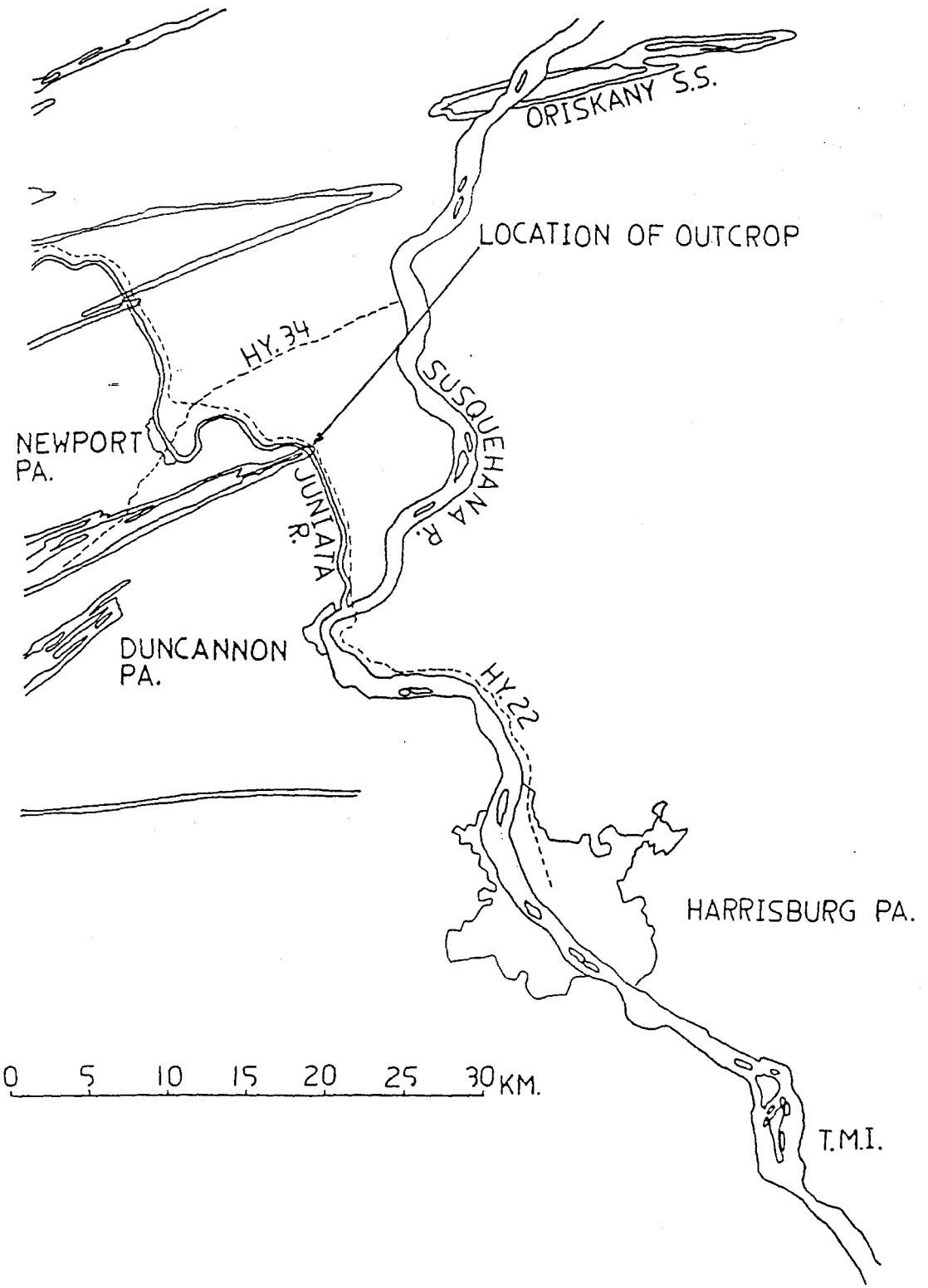
ORISKANY S.S.
LOCATION OF OUTCROP
HY. 34
SUSQUEHANNA R.
NEWPORT PA.
JUNIATA R.
DUNCANNON PA.
HY. 22
HARRISBURG PA.
T.M.I.
0 5 10 15 20 25 30 KM.

CHAPTER 2

2.1 Procedure

The sample suite is that of Buhay (1985). Samples were collected at three levels in the bed at eleven stations around the fold (see Fig. 8). (AC) sections were cut at stations 1, 2, 3, 5, 6, 8, and 11. In each section the C-axis orientations and poles to lamellae were measured for quartz grains containing lamellae using the universal stage. Data from each of the three sections at each station were rotated so as to bring the E-W direction of the stereonet coincident with bedding. The data were then combined, and contoured on equal-area projection (lower hemisphere) using the computer program of Robin and Jowett (1986) (see APPENDIX). The angular difference between C-axis orientation and pole to lamellae was also tabulated, and histograms were constructed which show the average crystallographic orientation of lamellae at each station. A composite histogram, accounting for a total of 446 sets of lamellae was also produced (see Fig. 11, p. 22-25).

An additional set of measurements was made in section A (top level) of stations 1, 2, 3, 6, 8, and 11. Here C-axis orientations of roughly 100 grains were taken, one half of which contained lamellae. Stereoplots of each were constructed, and contoured as above.

2.2 Limitations

There is an inherent limitation in the method of data collection. It arises due to the geometrical

Fig. 10 Limitations to method of data collection.

(a) "BLIND AREA" created as a result of being unable to see lamellae which are inclined at low angles to the plane of the thin section (p = pole to lamellae, C = C-axis orientation, L = lamellae orientation, (0001) = basal plane, t = plane of thin section). Poles to lamellae and C-axes for such lamellae fall within this blind area. It translates to the "central area" of stereoplot diagrams, of radius 45^{o}.

(b) Similar diagram showing the geometrical arrangement of C-axis, pole to lamellae, and basal plane for a set of lamellae inclined at a high angle to the plane of the thin section. Only lamellae of this sort are accounted for in this study. Poles and C-axes for these lamellae fall from 0^{o}-45^{o} to the plane of the thin section. This translates to the outer 45^{o} periphery of the corresponding steoeoplot diagrams.

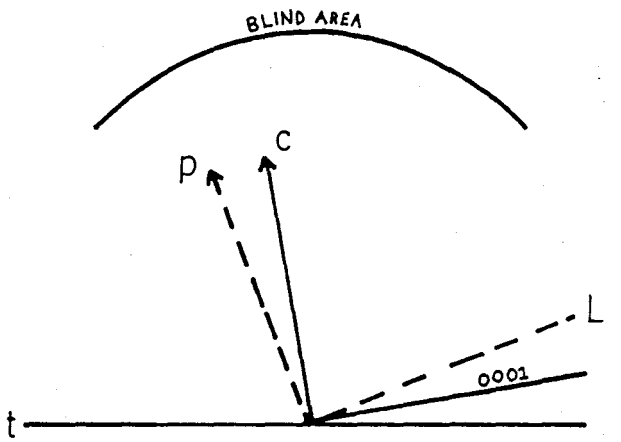

a

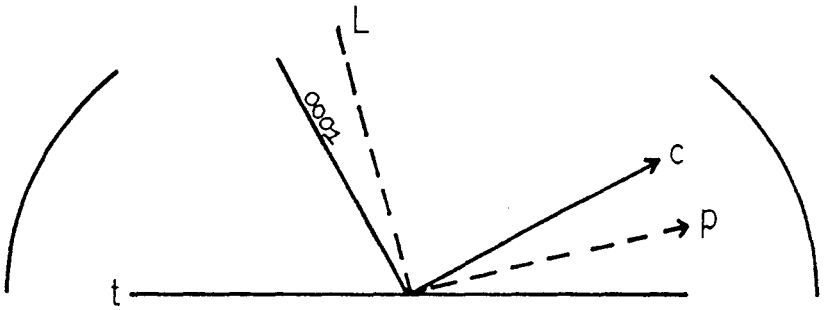

b

constraints imposed by measuring from one plane only, rather than from three mutually perpendicular planes. For example, those lamellae which are present in grains with C-axes which are at high angles to the plane of the thin section are statistically inclined at low angles to this plane. Using the universal stage it is impossible to rotate lamellae of these orientations into the viewing range of the optical microscope. As a result a "blind area" is created at the centre of the net where poles to such lamellae would otherwise fall (see Fig. 10).

Diagrams (a) and (b) of Fig. 12 verify this limitation. In each case a blind area of radius 40^{o}-45^{o} is present.

Unfortunately this limitation nullifies the significance of some of the "additional measurements" taken in the upper level at most stations. Here, C-axis fabrics of grains without lamellae should be regarded with reference to the outer regions of the diagram, ignoring data within the central area. Such a perspective must be taken because grains with C-axes in the central portion may indeed have contained lamellae, although they were not visible due to the geometrical constraints discussed above.

2.3 Description of Data

2.3.1 Histograms

Fig. 11 (p. 22-25) shows the histograms constructed for each station, as well as the composite histogram. Of those constructed for separate stations, four of six show a

Fig. 11 Histograms: 1, 2, 3, 5, 6, 8 and 11 are histograms for separate stations. The last (p. 25) is a composite histogram for a total of 446 measurements of lamellae sets across the fold.

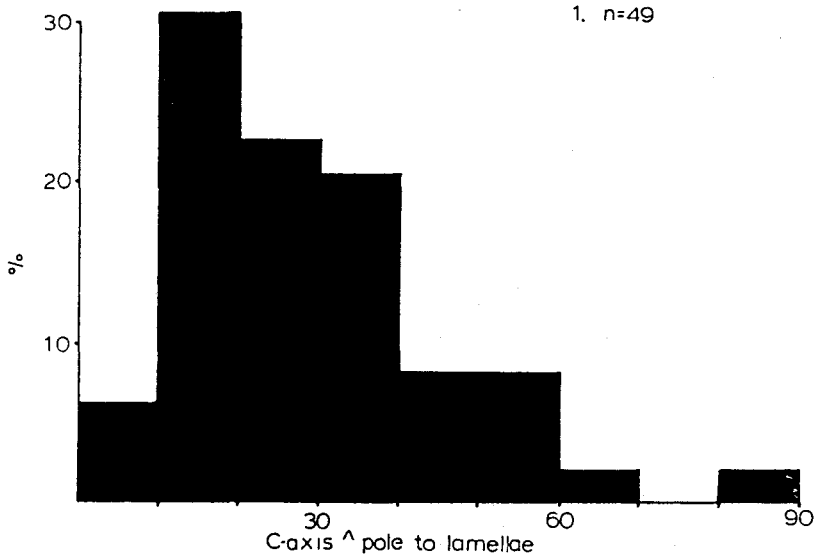
1. n=49
30
20
10
%
30
60
90
C-axis ^ pole to lamellae

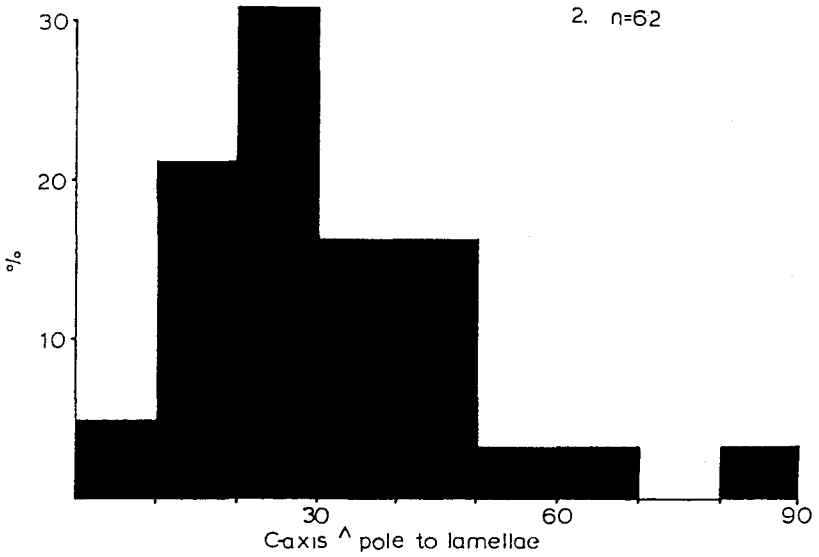
2. n=62
30
20
10
%
30
60
90
C-axis ^ pole to lamellae

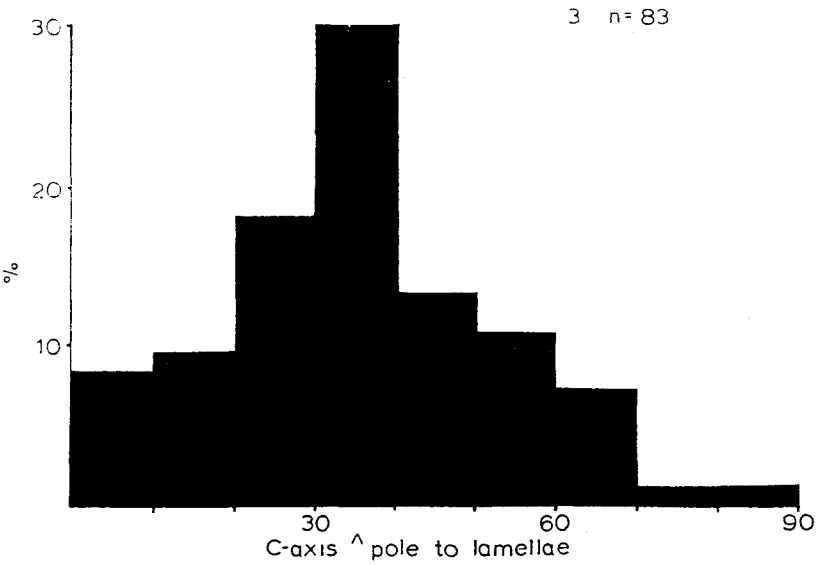
3 n=83
30
20
10
%
30
60
90
C-axis ^ pole to lamellae

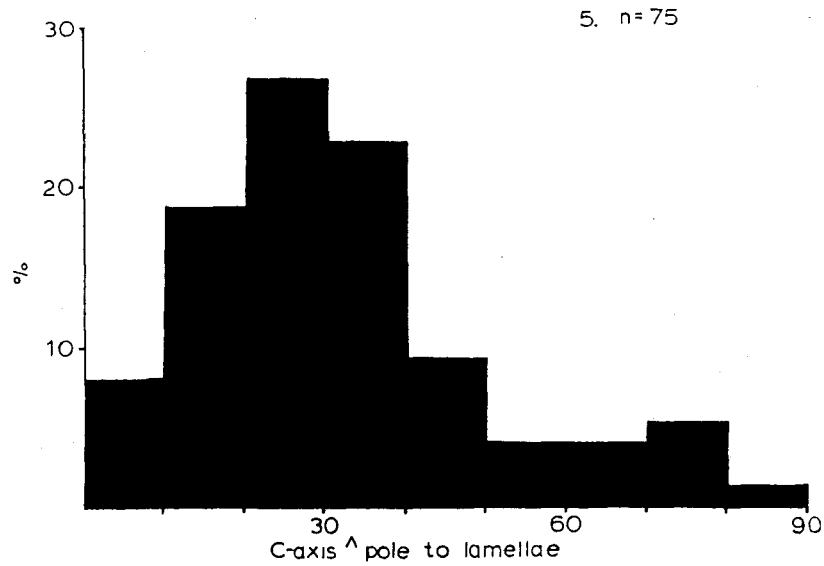
5. n=75
30
20
10
%
30
60
90
C-axis ^ pole to lamellae

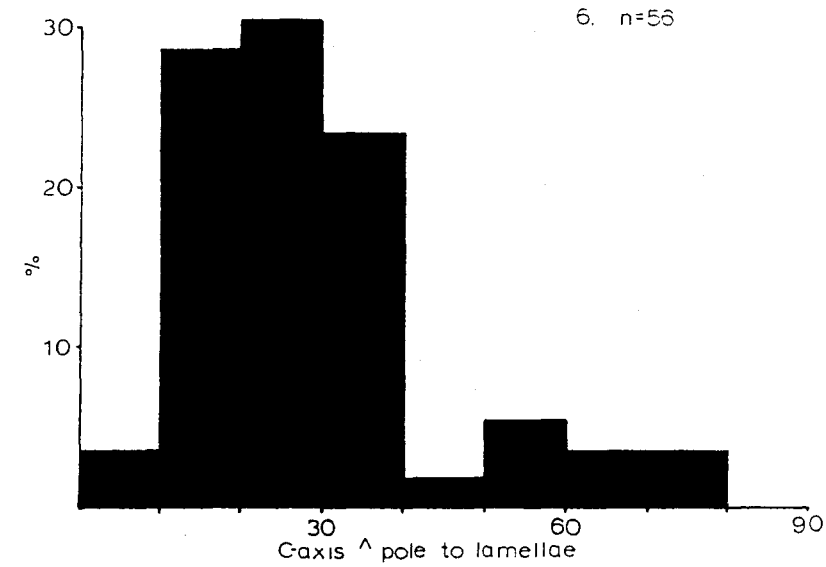
6. n=56
30
20
10
%
30
60
90
C-axis ^ pole to lamellae

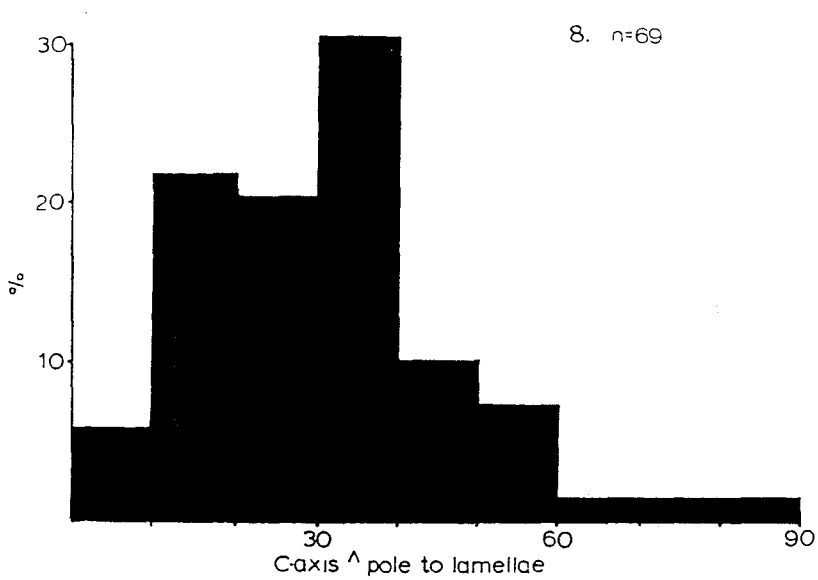
8. n=69
30
20
10
%
30
60
90
C-axis ^ pole to lamellae

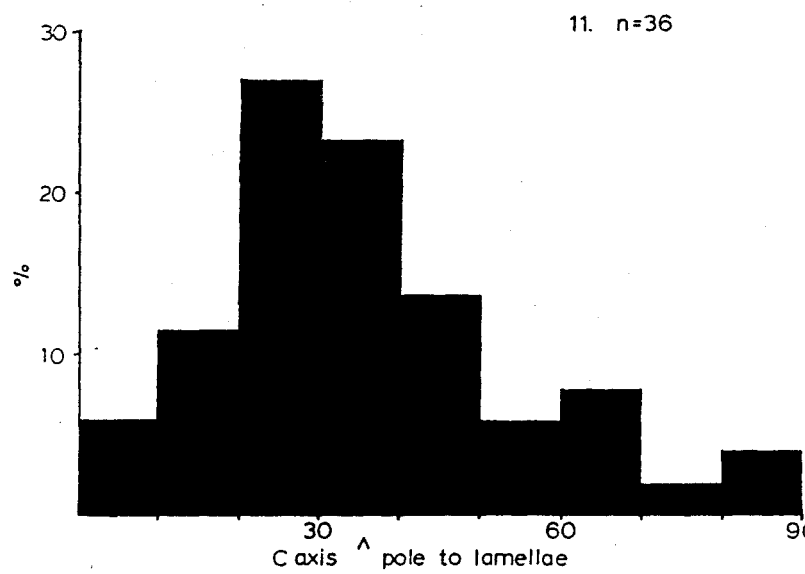
11. n=36
30
20
10
%
30
60
90
C axis ^ pole to lamellae

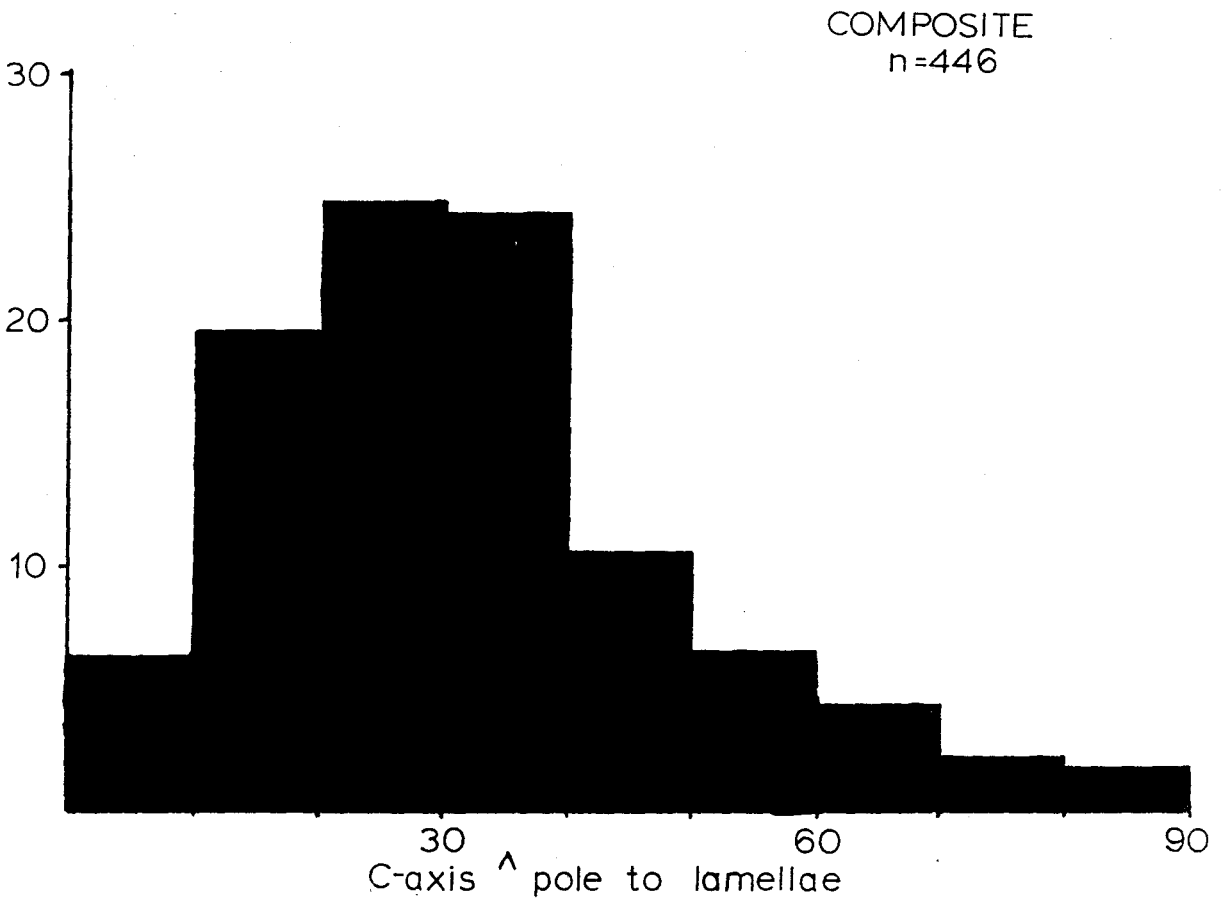
COMPOSITE
n=446
30
20
10
30
60
90
C-axis ^ pole to lamellae

mode in the interval of 20^{o}-30^{o} from the C-axis. In addition, all generally show the highest proportion of lamellae in the 10^{o}-45^{o} interval. The composite displays the same trends; its mode is in the 20^{o}-30^{o} interval while most lamellae fall in the 10^{o}-45^{o} range.

2.3.2 Data for Separate Stations

Three diagrams have been constructed, in all cases labelled (a), (b), and (c) (Fig. 12, p. 31-41). Diagram (a) is a contoured stereoplot of poles to lamellae in an average of 70 grains. (b) is likewise a contoured diagram. It shows the C-axis orientations of the grains containing lamellae above. (c) is referred to as an arrow diagram. It displays arrows which join the C-axis (tail) to pole (head) of the grains above. Its usefulness is in determining stress directions, as discussed in section 1.4 (p. 14). Only angular intervals of 5^{o}-40^{o} between C-axis and pole are included.

STATION 1 (Fig. 12, p. 31-32)

(a) Poles to lamellae show four maxima. All fall along a small circle girdle of radius 60^{o} whose centre is at the centre of the net. Two are more strongly defined; these lie in the northwest and southeast quadrants. Lines joining maxima in opposite quadrants define acute and obtuse bisectrices of the plot; by inversion these define the acute and obtuse bisectrices for the mean orientations of lamellae. In this case these are 60^{o} and 120^{o} respectively.

(b) Contoured C-axes of grains containing lamellae display five maxima. These also lie on a small circle whose centre is at the centre of the net. In this case the small circle radius is 70^{o}-80^{o}. The angle between maxima in the upper quadrants is 60^{o} while the angle between maxima in the lower quadrants is 85^{o}. An

approximate value for the acute bisectrix is therefore 70^{o}.

(c) The bulk of arrows connecting C-axes (tails) to poles (heads) point away from bedding with the exception of those in the northwest quadrant; here, the majority point towards bedding. Mutually perpendicular lines x and y are drawn so as to define the symmetrical distribution of arrow trends in each quadrant. These groupings are most likely related to stress orientations, as will be discussed in section 3.6.4. In this case x is roughly bedding parallel.

STATION 2 (Fig. 12, p. 32-33)

(a) Poles to lamellae show three large maxima, two in the southeast quadrant and one in the northeast. These define an incomplete small circle girdle of radius 70^{o} whose centre is at the centre of the net. The angle between maxima in the upper quadrants is 55^{o}, defining the acute bisectrix. By geometry, the obtuse bisectrix is therefore 125^{o}.

(b) The C-axis fabric of grains containing lamellae is characterized by pronounced maxima in the northwest and southeast quadrants accompanied by more diffuse maxima in adjacent quadrants. Data generally lie within 10^{o}-20^{o} of the periphery of the diagram and can be joined along the great circle which forms its primitive. Obtuse and acute bisectrices are also definable; the former is given by the angle between maxima in the upper quadrants which is 94^{o}. The latter is given by the angle between maxima in quadrants of opposing halves of the diagram. It is 86^{o}.

(c) The majority of arrows in the southwest quadrant point away from bedding, as do those in the northeast quadrant. In the northwest and southeast arrows are directed from the periphery to the inner region of the net. In this case mutually perpendicular lines x and y (lines dividing "symmetrical" arrow groupings) are displaced with respect to bedding by 20^{o} in a counterclockwise direction.

STATION 3 (Fig. 12, p. 34-35)

(a) Poles to lamellae display four maxima. All are joinable along the trend of a small circle of radius 60^{o} whose centre is at the centre of the diagram. In addition, the maxima may define two further small circles. One connects data in the upper quadrants; it has a radius of 40^{o} and a centre situated at 9^{o} west of north. The other connects the more pronounced maxima of the southwest and southeast quadrants; its

radius is 45° while its centre is at 13° east of south. The acute bisectrix is given by the average apical angle of the cones defined by these circles. It is 80°-85°.

(b) The C-axis orientations display a symmetrical pattern of four maxima, one in each quadrant. Maxima can be joined along the trace of the great circle forming the boundary of the diagram. The acute bisectrix is 85° while the obtuse bisectrix is 95°. All maxima are oriented at roughly 45° to bedding.

(c) The arrow diagram shows similar trends to those of station 2. In the southwest and northwest quadrants arrows generally point away from bedding. A more complex pattern is seen in the northwest; here, arrows are oriented randomly with respect to one another and no general pattern is visible. In the southeast quadrant arrows point from the peripheral to inner regions of the plot. The two mutually perpendicular lines x and y are offset with respect to bedding by about 20° in a counterclockwise direction.

STATION 5 (Fig. 12, p. 35-36)

(a) Three significant maxima are given by poles to lamellae. Two are located at approximately 40°-60° to bedding in the northwest and southwest quadrants. The other is located 8° east of north. The acute bisectrix, given by the angle between maxima in the upper quadrants, is 50°. All maxima can be joined along a small circle of radius 65° about the centre of the net.

(b) The C-axis fabric of grains containing lamellae shows maxima in each of the four quadrants. Three of the four are inclined at 45°-65° to bedding. The acute and obtuse bisectrices, as derived from lines connecting maxima in opposite quadrants, are 83° and 97° respectively. All maxima fall at the edge of the diagram, and can be connected via the great circle which forms its boundary.

(c) Arrows show a more pronounced directional trend in the southwest quadrant, and in the north-northeast. In both cases, arrows point away from bedding. The bulk of arrows in the northwest quadrant point from the outer edge to the inner portion of the diagram. Scattered arrows on the east and southeastern boundaries show a similar directional pattern. Lines x and y are offset with respect to the east-west and north-south axes of the diagram by a small angle in a counterclockwise direction.

STATION 6 (Fig. 12, p. 37-38)

(a) Poles to lamellae display 3 maxima, two of which are situated at 74^{o} to each other in the lower quadrants, and one which stretches across the upper periphery of the diagram. The angular difference between the orientation of the former two can be taken as a rough approximation of the acute bisectrix. All maxima lie along the trend of a small circle of similar radius and orientation to those of stations 1, 2, and 5.

(b) Four maxima are present, one in each of the four quadrants. All lie along the great circle which forms the boundary of the diagram. The obtuse bisectrix is 96^{o} while the acute bisectrix is 84^{o}. Each of the maxima lie at roughly 45^{o}-65^{o} to bedding.

(c) In each quadrant the majority of arrows point away from bedding, and towards the north or south of the diagram respectively. Lines x and y are not offset with respect to the east-west and north-south directions of the diagram.

STATION 8 (Fig. 12, p. 38-39)

(a) Poles to lamellae display four maxima. The two in the upper half of the diagram lie along a small circle girdle of radius 35^{o} whose apex is at 10^{o} east of north. The apical angle of the cone of this girdle is 66^{o}, which can be taken as in approximate value for the acute bisectrix. Such a value corresponds closely to the angle between maxima in the lower quadrants, which is 66^{o}. An incomplete small circle girdle in the plane of the diagram is less well defined in this case.

(b) The C-axis orientations define four maxima; two are more pronounced and lie in the northeast and southwest quadrants while two are diffuse and lie in adjacent quadrants. All lie within 20^{o}-30^{o} of the outer edge of the diagram. As such three define an incomplete small circle girdle of radius 75^{o} whose centre is near the centre of the diagram. The acute and obtuse bisectrices are 77^{o} and 103^{o} respectively.

(c) Arrows in the southwest quadrant point away from bedding, as do those in the southeast. In the upper two quadrants arrows show similar trends. Lines x and y are offset with respect to the east-west and north-south axes of the diagram by a small angle in the clockwise direction.

STATION 11 (Fig. 12, p. 40-41)

(a) Poles to lamellae show one large maximum near the eastern boundary accompanied by several diffuse maxima scattered throughout the diagram. All can be joined along a small circle of radius 70^{o} whose centre is at the centre of the plot.

(b) Contoured C-axes define two large maxima on the west and east sides of the diagram; these are above and below the orientaion of bedding respectively and are symmetrically disposed with respect to one another. A more diffuse maxima is located 20^{o} east of north.

(c) The most concentrated assemblage of arrows occurs on the eastern side of the diagram, coincident with maxima for C-axes and poles of diagrams (a) and (b). Lines x and y again divide the diagram into four quadrants based on trends of arrow direction; arrows in the northwest and northeast generally point towards the north, while those in the southeast and southwest point towards the south. Lines x and y are offset with respect to the north-south and east-west axes of the diagram by roughly 25^{o} in a clockwise direction.

Summary

(a) Poles to lamellae generally show three to four maxima. In almost every case these may be joined to form an incomplete small circle girdle of radius 60^{o}-70^{o} about the centre of the diagram. Lines joining maxima in opposite quadrants are of relatively consistent orientation; they usually define the acute bisectrix as the angle between maxima in the upper quadrants and the obtuse bisectrix as the angle between maxima in adjacent quadrants of the upper and lower halves of the diagram. These geometrical relationships are portrayed in Fig. 13(a). An average value for the acute bisectrix is 60^{o}. At two stations (3 and 8) maxima in either of the upper or lower quadrants lie along the trend of a small circle girdle whose centre is near the North or South of the diagram (see Fig. 13(b)).

Fig. 12 Data for separate stations. Three diagrams are displayed for each station. They are:

(a) poles to quartz lamellae
(b) C-axis orientations of grains containing lamellae
(c) Arrow diagrams; arrows connect C-axes (tails) to poles (heads) of grains above.

For all diagrams, K = 100. Contours for (a) and (b) are E+2, E+4, E+8 . . . E+12 sigma. N, E and sigma values for each diagram are given below. For the arrow diagrams, only N is given.

Station 1 (p. 31-32)

(a) N = 50, sigma = 0.49, E = 0.50
(b) N = 49, sigma = 0.49, E = 0.49
(c) N = 37

Station 2 (p. 32-33)

(a) N = 62, sigma = 0.55, E = 0.62
(b) N = 62, sigma = 0.55, E = 0.62
(c) N = 44

Station 3 (p. 34-35)

(a) N = 83, sigma = 0.64, E = 0.83
(b) N = 83, sigma = 0.64, E = 0.83
(c) N = 42

Station 5 (p. 35-36)

(a) N = 76, sigma = 0.61, E = 0.76
(b) N = 75, sigma = 0.61, E = 0.75
(C) n = 55

Station 6 (p. 37-38)

(a) N = 56, sigma = 0.52, E = 0.56
(b) N = 56, sigma = 0.52, E = 0.56
(c) N = 47

Station 8 (p. 38-39)

(a) N = 69, sigma = 0.58, E = 0.69
(b) N = 69, sigma = 0.58, E = 0.69
(c) N = 53

Station 11 (p. 40-41)

(a) N = 53, sigma = 0.51, E = 0.53
(b) N = 54, sigma = 0.51, E = 0.54
(c) N = 32

1a

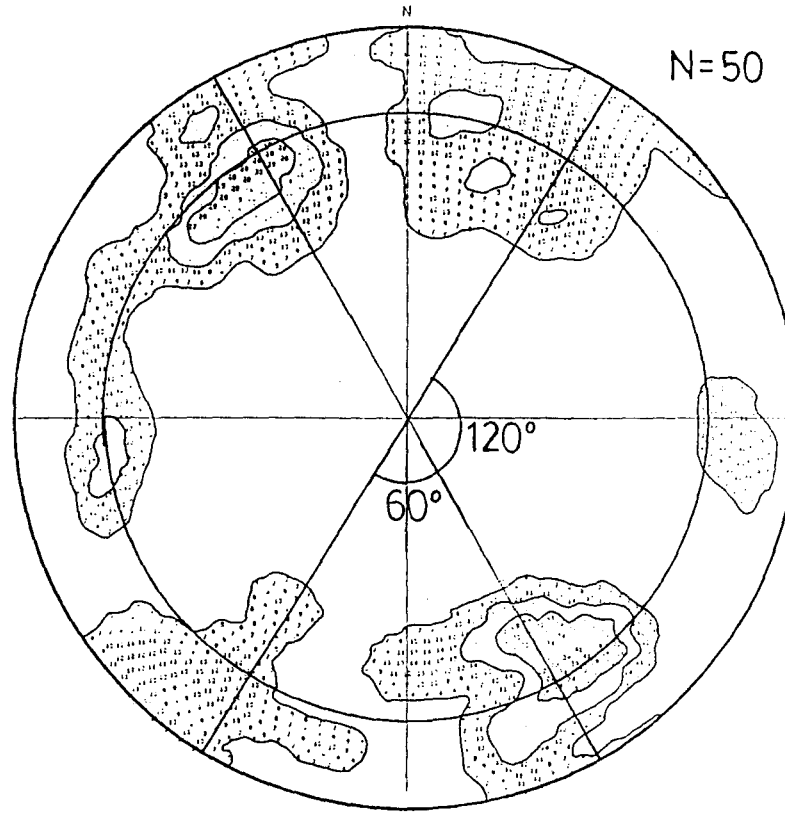

1b

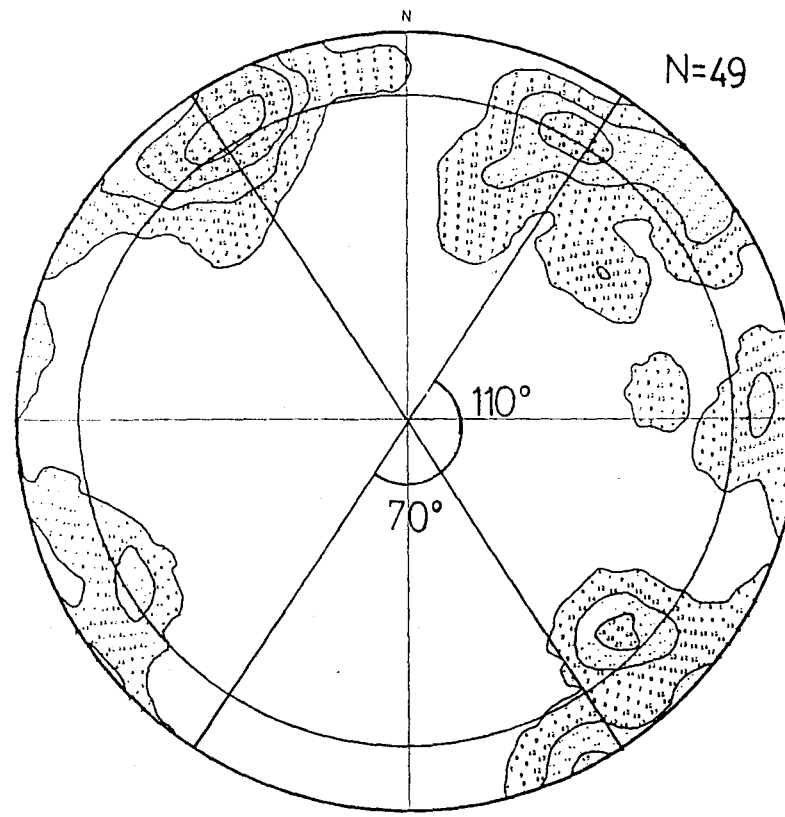

1c

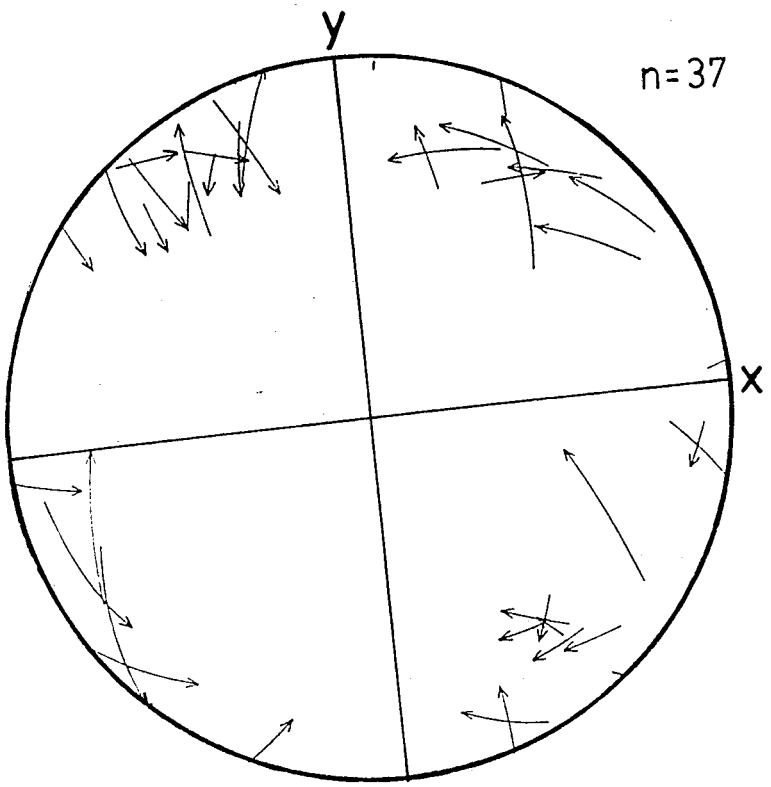

2a

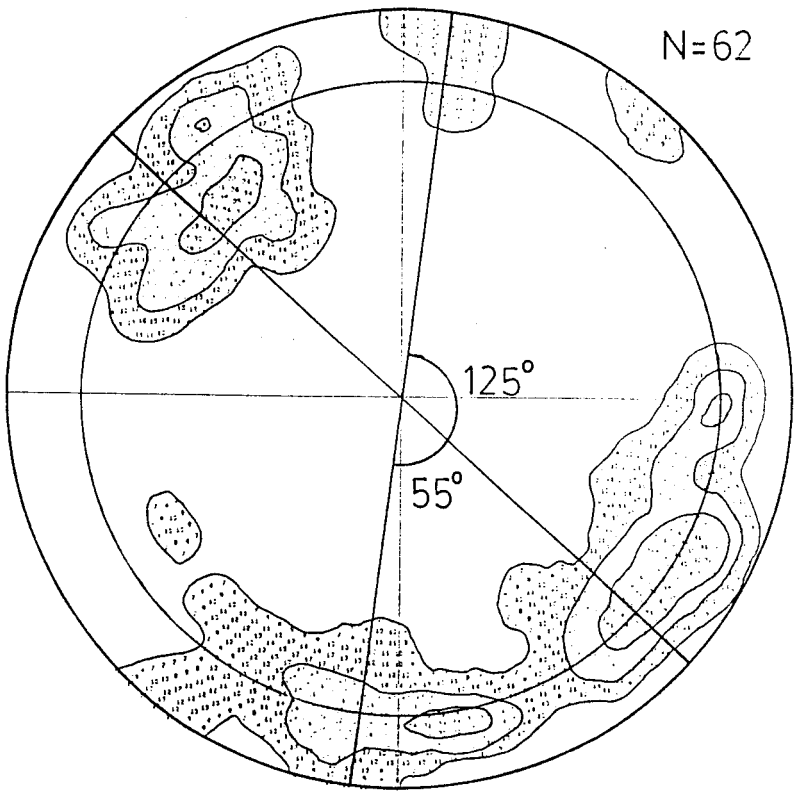

2b

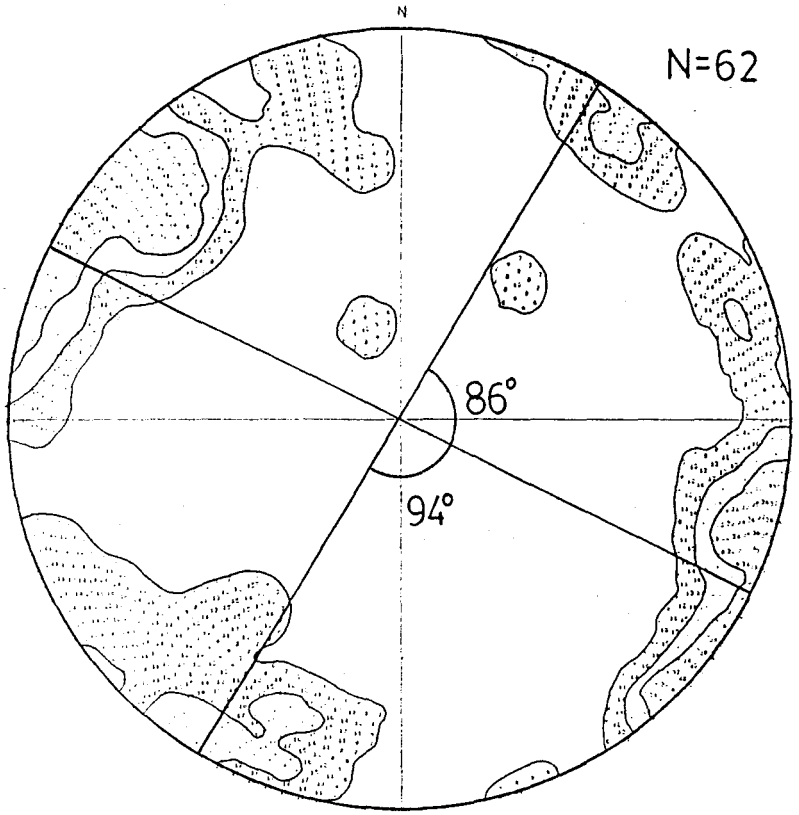

2c

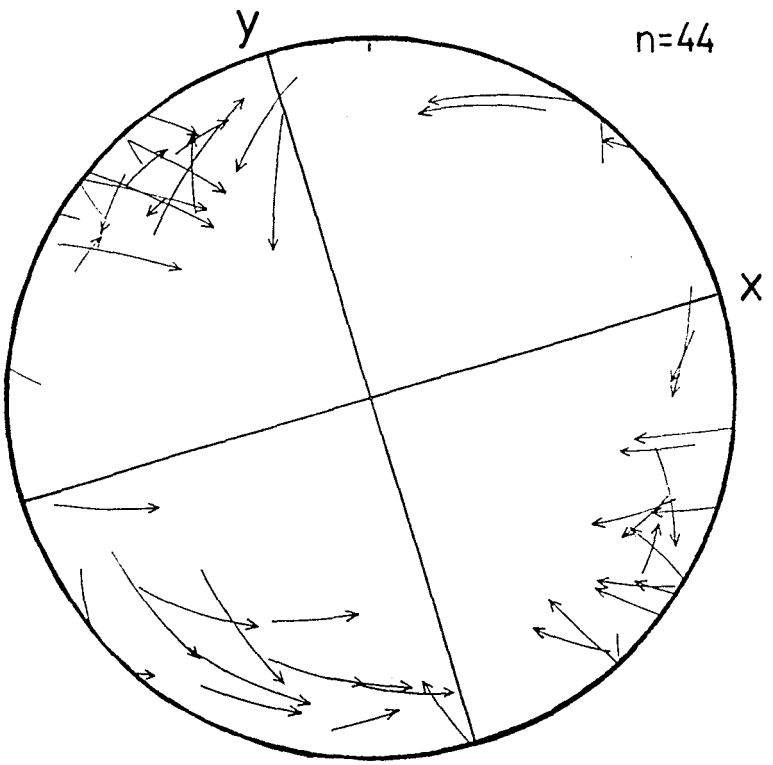

3a

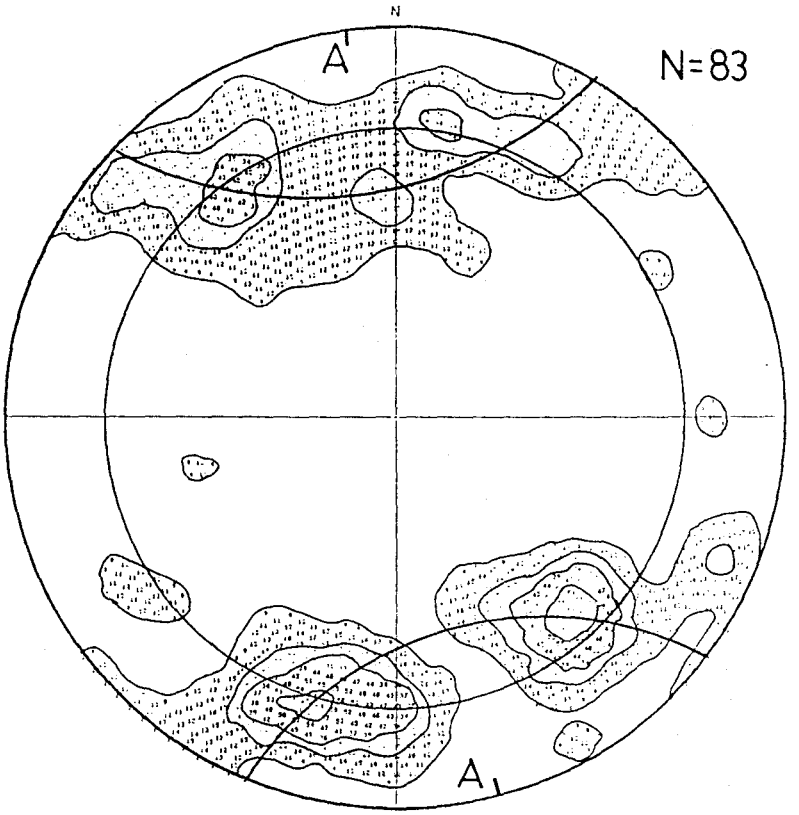

3b

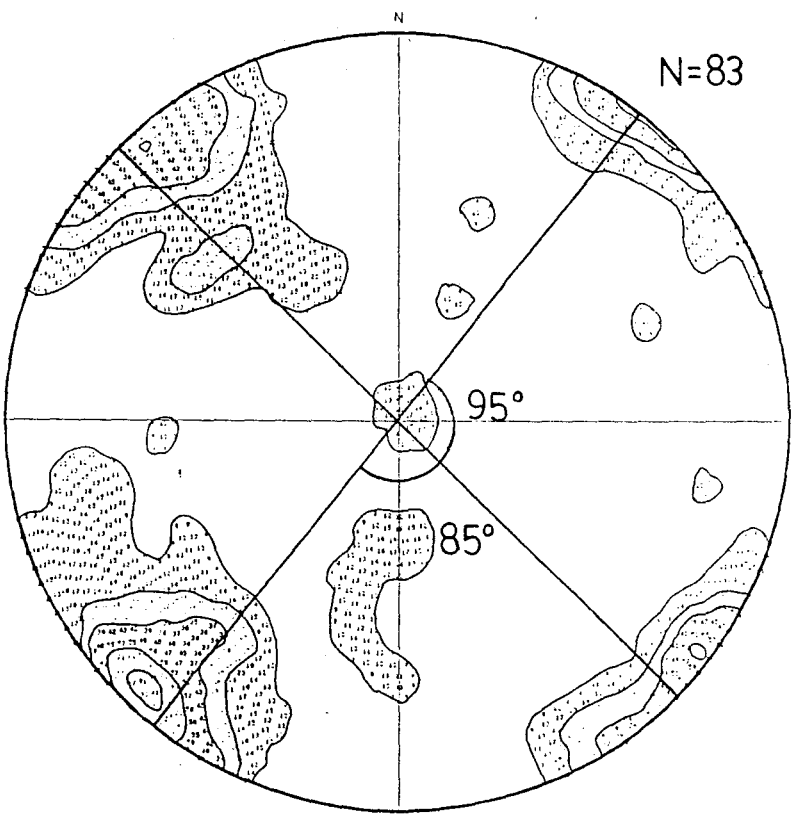

3c

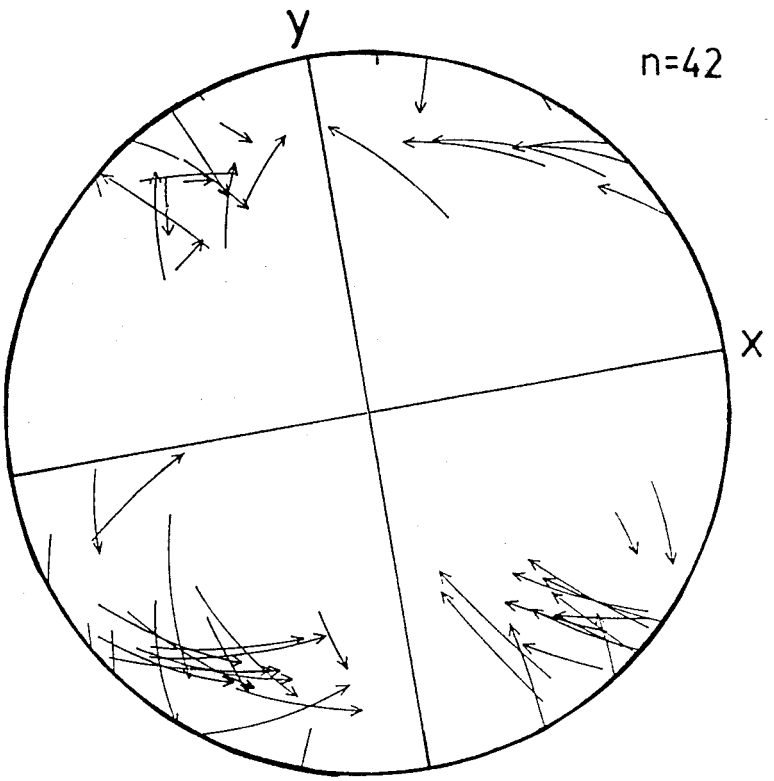

5a

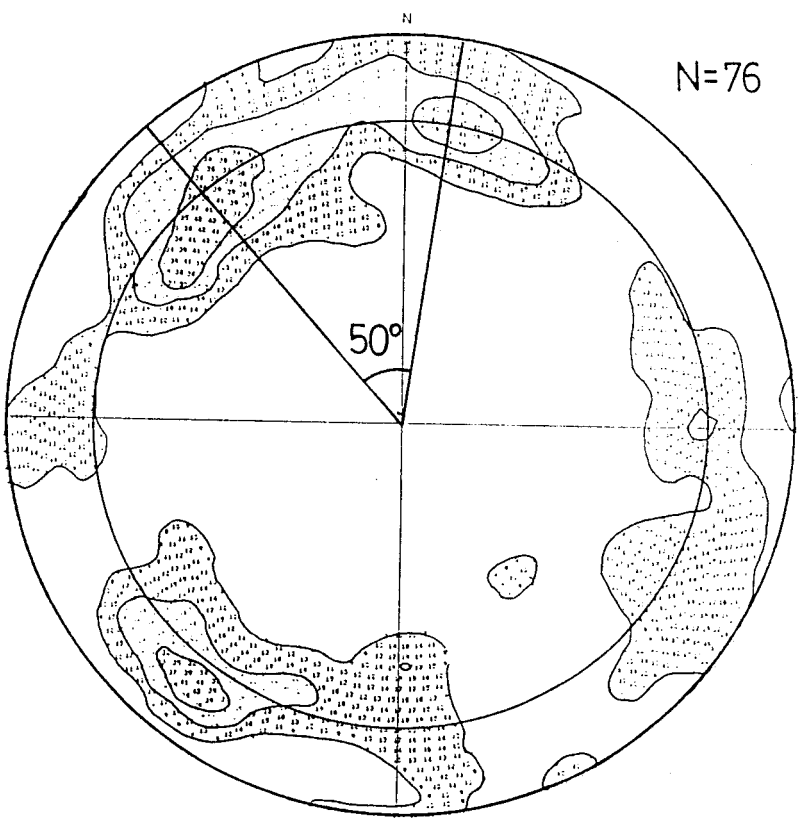

5b

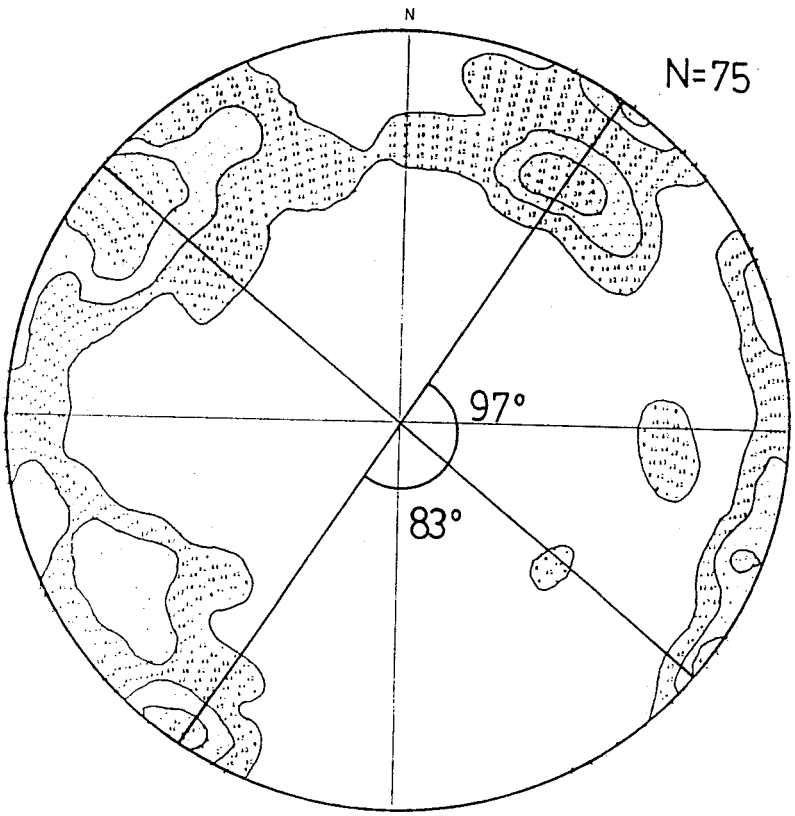

5c

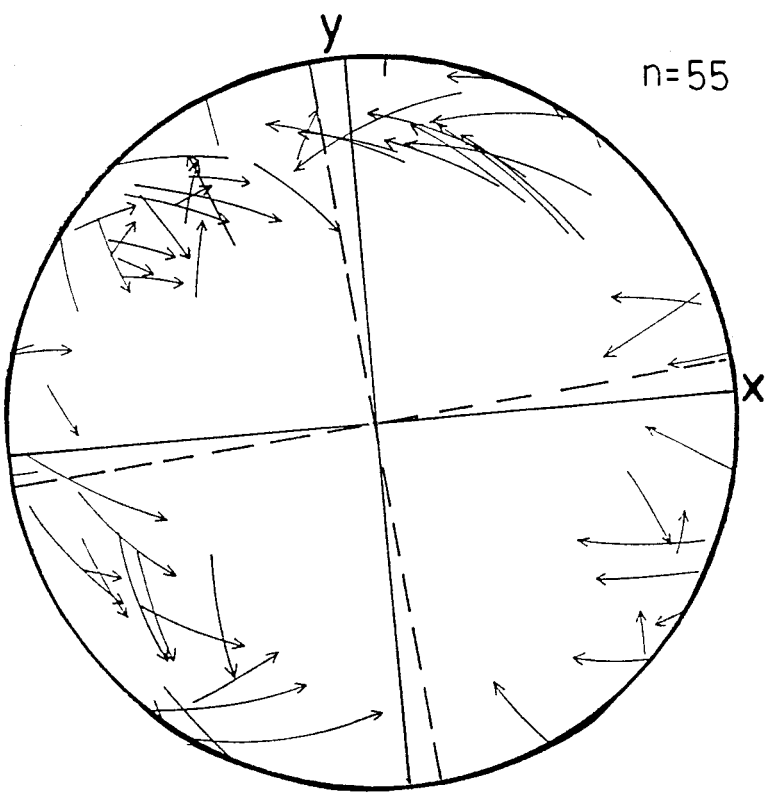

6a

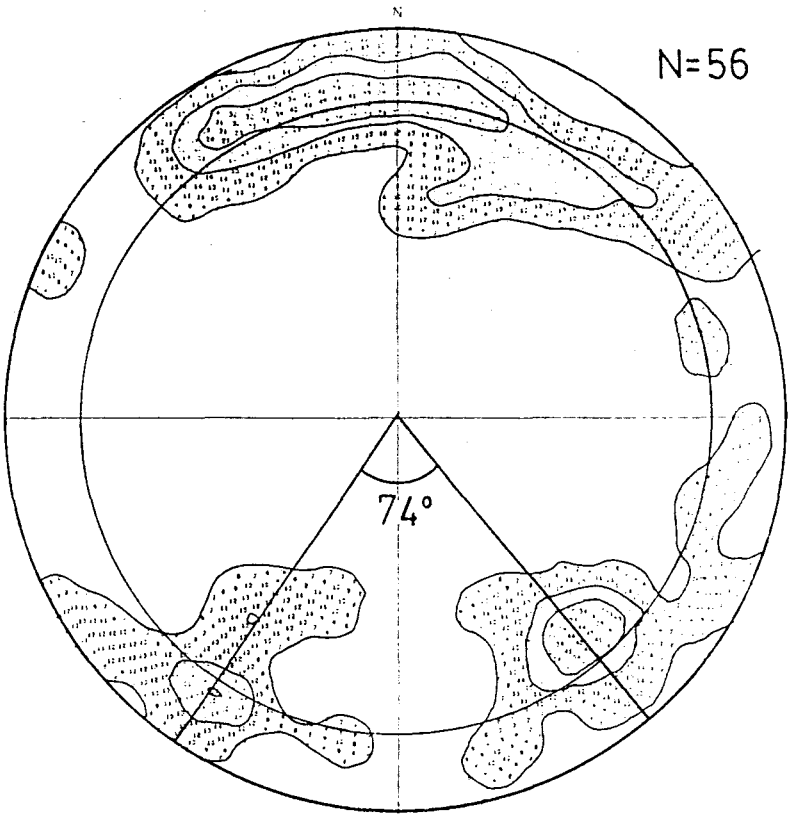

6b

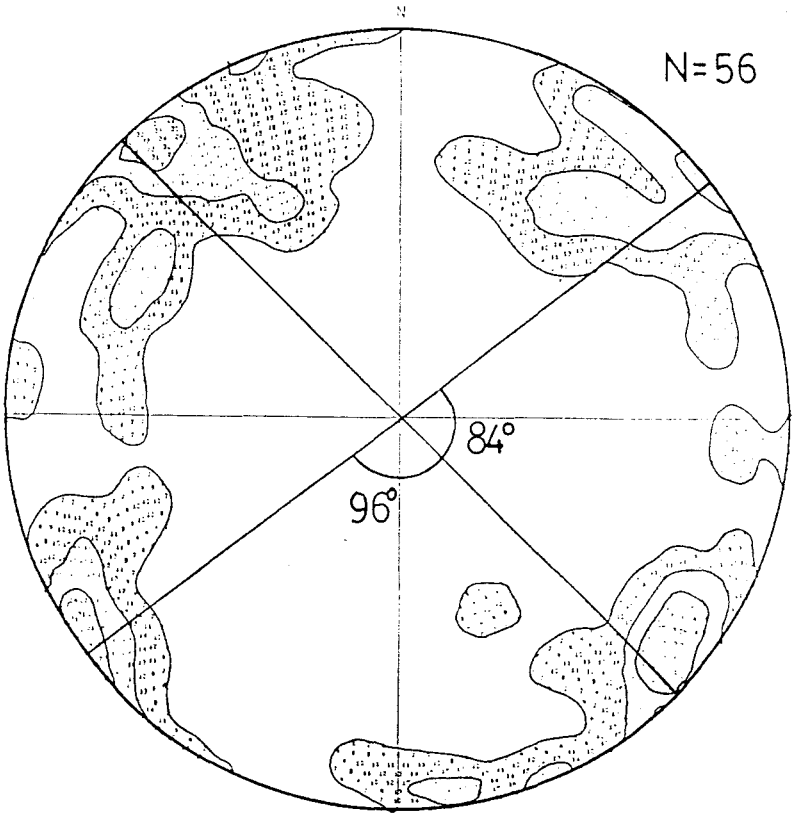

6c

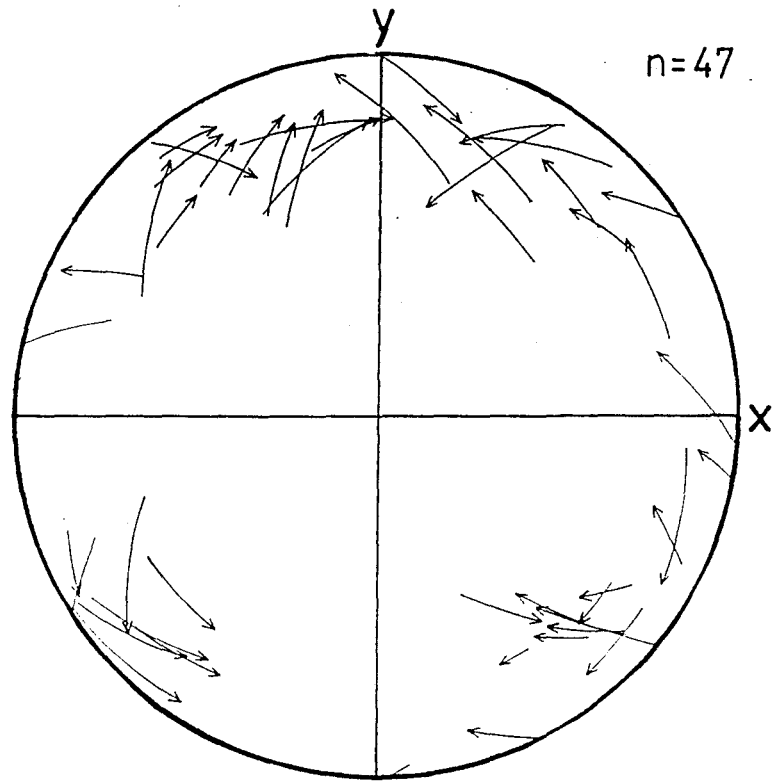

8a

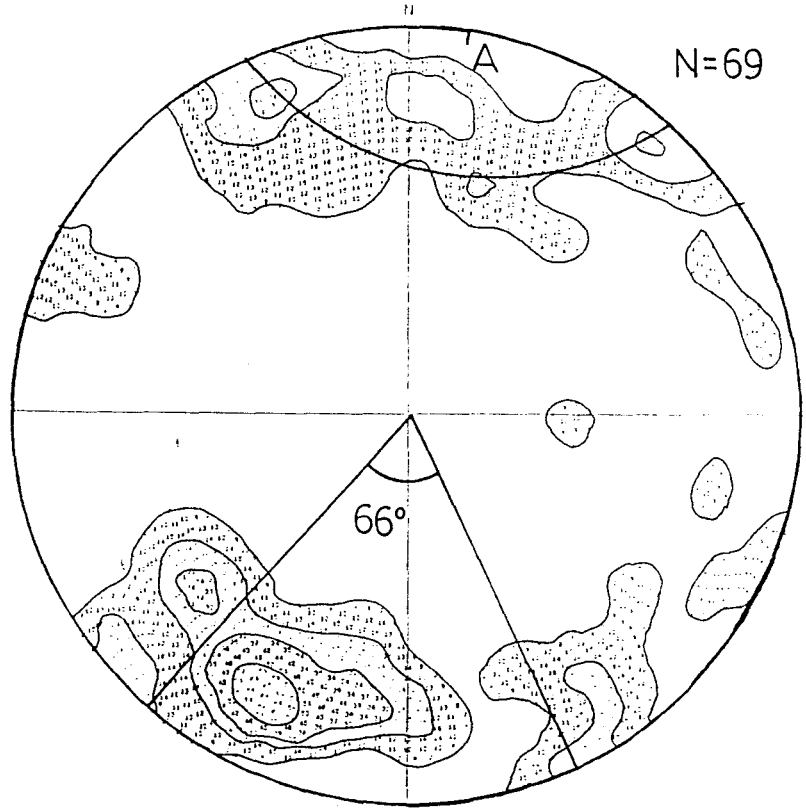

8b

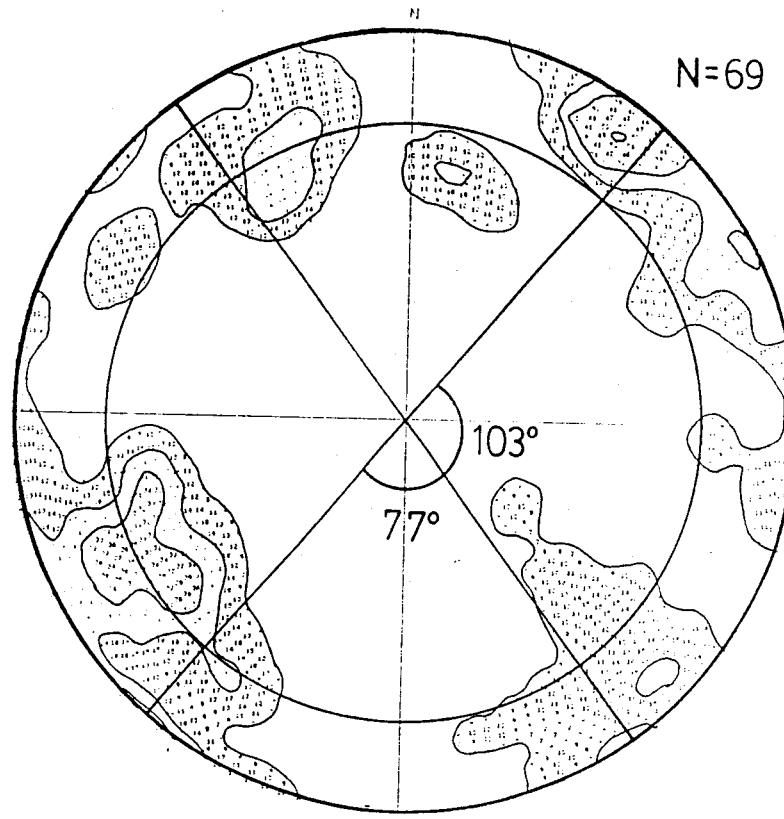

8c

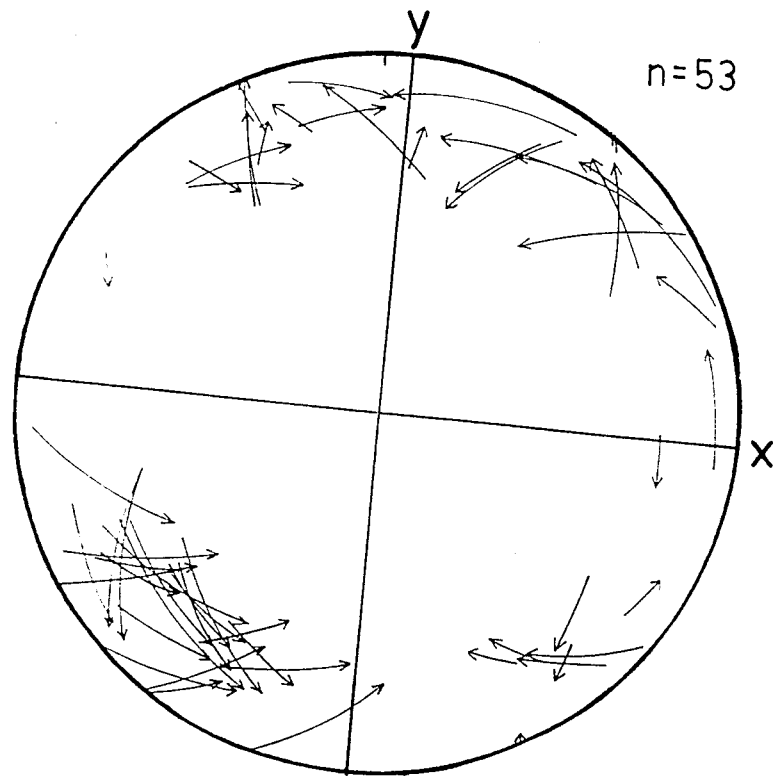

11a

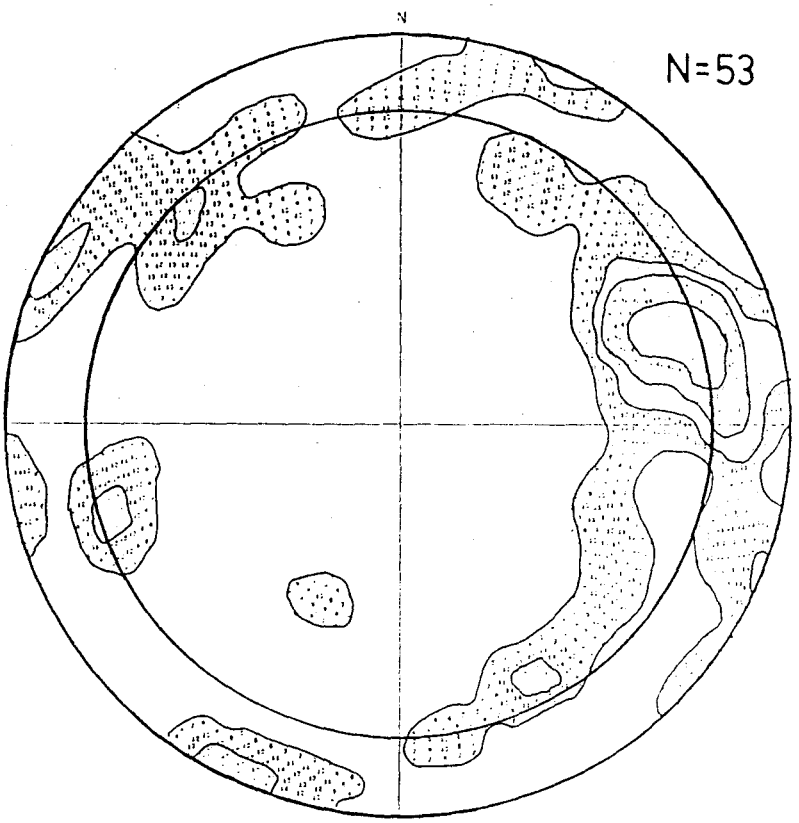

11b

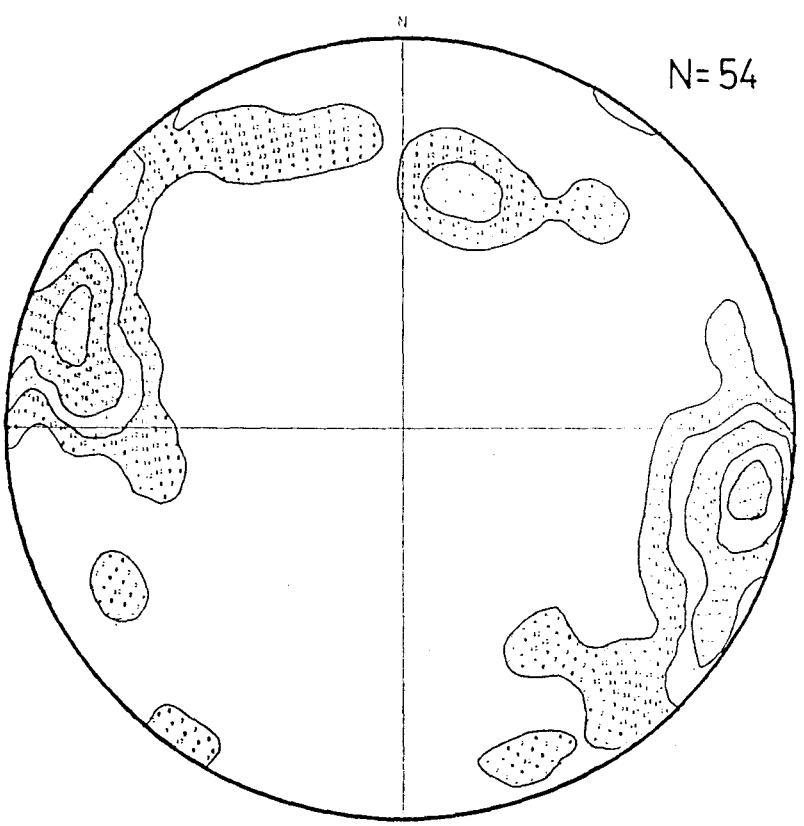

11c

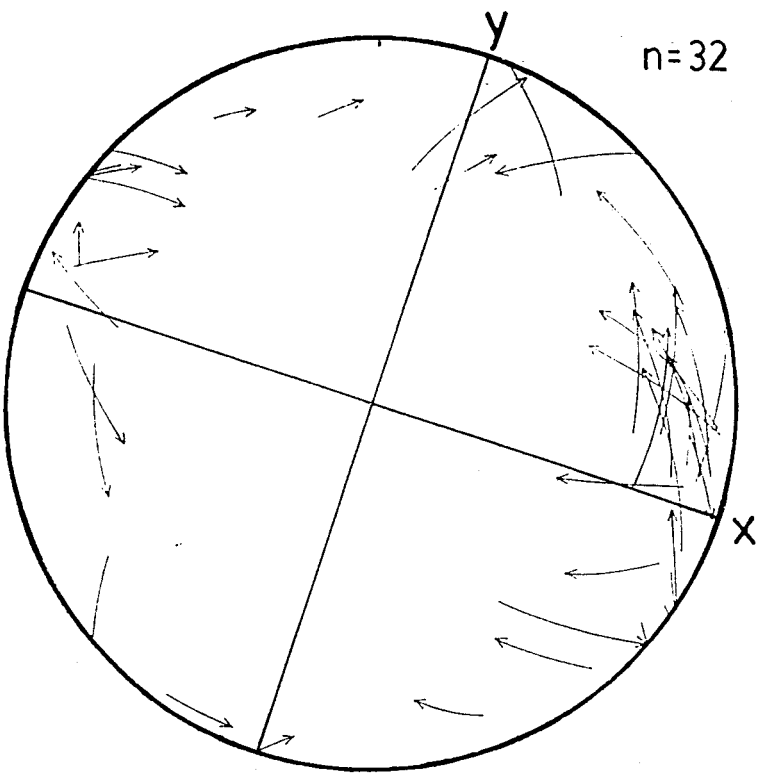

It is debatable as to whether maxima which have otherwise been interpreted as "independent" positions may be defined as forming incomplete small circle girdles of similar orientations (see question mark, Fig. 13(b)).

Fig. 13(a) and (b) represent "average" geometrical arrangements. In reality the four maxima and the distribution lines which join them may be rotated clockwise or counterclockwise with respect to the north-south direction of the diagram. At stations 2, 3, and 5 this average grid is skewed in a counterclockwise direction while at stations 11 and 8 it is skewed in a clockwise direction. At stations 1 and 6 it remains at the position portrayed. These shifts in position follow the pattern of shifts for the arrow diagrams. This is to be expected since the arrow diagrams involve use of the same data.

(b) C-axes also display three to four maxima. These are most often situated near the edge of the diagram at 40^{o}-60^{o} to bedding, one in each of the four quadrants (see Fig. 13(c)). Acute and obtuse bisectrices are each generally close to 90^{o}.

(c) Arrows in the northeast and southwest quadrants consistently point away from bedding towards the north and south of the diagram respectively. Arrows in the northwest and southeast show more variable patterns of direction. At some stations (3, 5, 2) they show a pronounced trend in direction from the outer edge to the inner region of the

Fig. 13 (a, b). "Average" geometrical arrangement of poles to quartz lamellae across fold. (c). "Average" geometrical arrangement of C-axes of grains containing lamellae across fold.

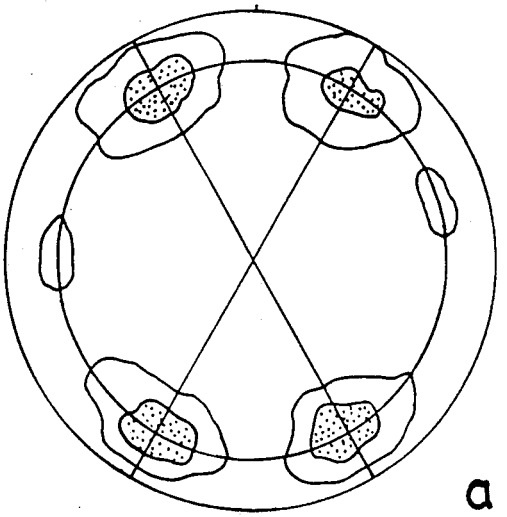

a

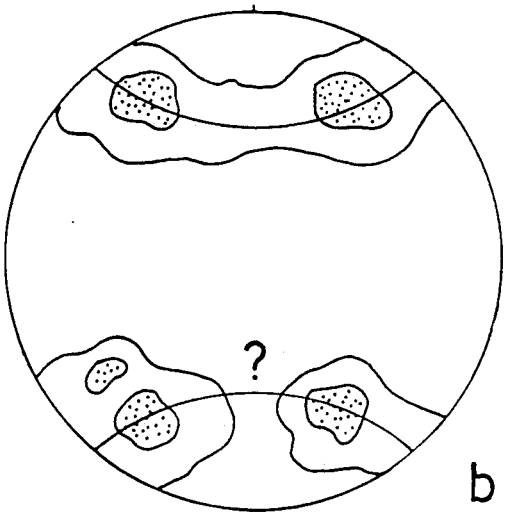

b

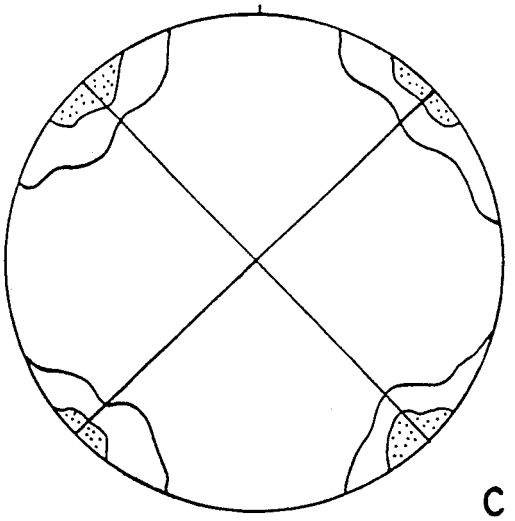

c

diagram; at others (8, 11), a good portion point away from bedding in a similar manner to those of the northeast and southwest quadrants. Yet in others, a mixture of the two trends is apparent (1, 6).

At stations 2, 3 and 5 lines x and y are offset with respect to the north-south and east-west directions of the diagram in a counterclockwise direction. At stations 1 and 6, x and y are not offset with respect to these directions, and at stations 8 and 11 they are offset in a clockwise direction.

2.3.3 Additional Measurements

Fig. 14 (p. 46-51) shows data collected in section A (upper level) of stations 1, 2, 3, 6, 8 and 11. Two plots were constructed for each; one displays C-axis orientations of roughly 50 random grains containing lamellae (in all cases labelled (a)); the other displays C-axis orientations of another 50 random grains without lamellae (in all cases labelled (b)). The latter must be regarded with respect to the outer 40^{o} portion of the diagram in accordance with the limitations described in section 2.2.

At all stations the C-axis fabrics of grains containing lamellae are less random in their distribution than the equivalent fabrics of grains without lamellae. In particular, the majority of well-defined maxima occur in diagrams of category (a). The maxima are also more often than not situated in one of the four quadrants at roughly

45° to bedding (note, for e.g., diagrams 6(a), 3(a), and 8(a)). An additional observation is that there is no obvious correspondence in fabric as between diagrams (a) and (b), in each case.

Fig. 14 Additional Measurements; Stations 1, 2, 3, 6, 8 and 11. Diagram (a) displays C-axis orientations of grains containing lamellae. Diagram (b) displays C-axis orientations of grains without lamellae. For all diagrams, K = 100. Contours are E+2, E+4, E+8 . . . E+12 sigma. N, E and sigma values are given below.

Station 1 (p. 46)

(a) N = 60, sigma = 0.54, E = 0.60
(b) N = 61, sigma = 0.55, E = 0.61

Station 2 (p. 47)

(a) N = 51, sigma = 0.50, E = 0.51
(b) N = 49, sigma = 0.49, E = 0.49

Station 3 (p. 48)

(a) N = 60, sigma = 0.54, E = 0.60
(b) N = 49, sigma = 0.49, E = 0.49

Station 6 (p. 49)

(a) N = 72, sigma = 0.62, E = 0.79
(b) N = 86, sigma = 0.65, E = 0.86

Station 8 (p. 50)

(a) N = 58, sigma = 0.53, E = 0.58
(b) N = 51, sigma = 0.50, E = 0.51

Station 11 (p. 51)

(a) N = 54, sigma = 0.51, E = 0.54
(b) N = 52, sigma = 0.50, E = 0.52

1a

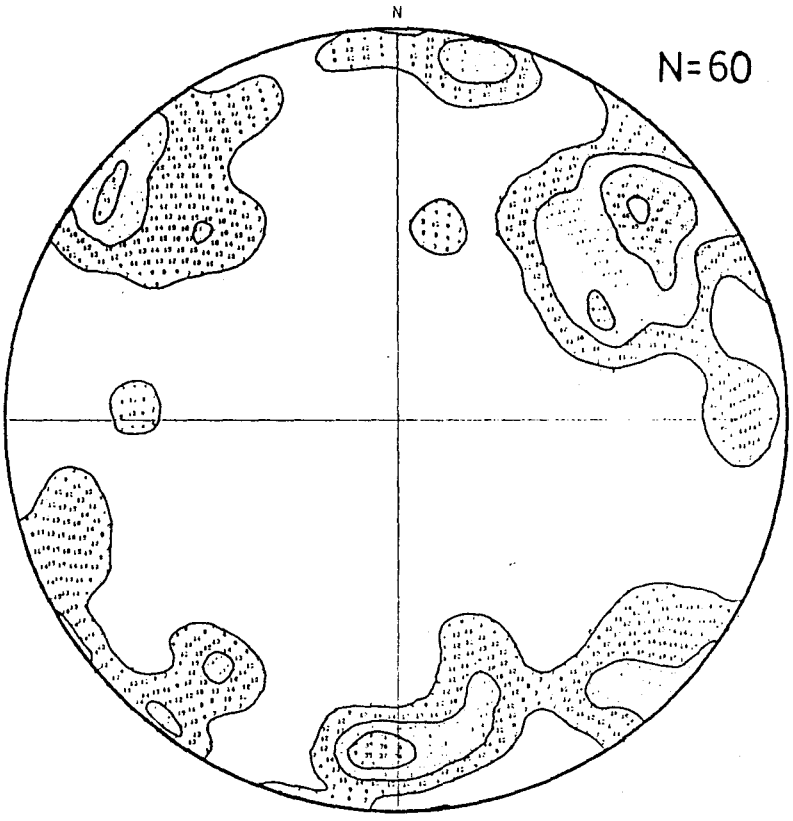

1b

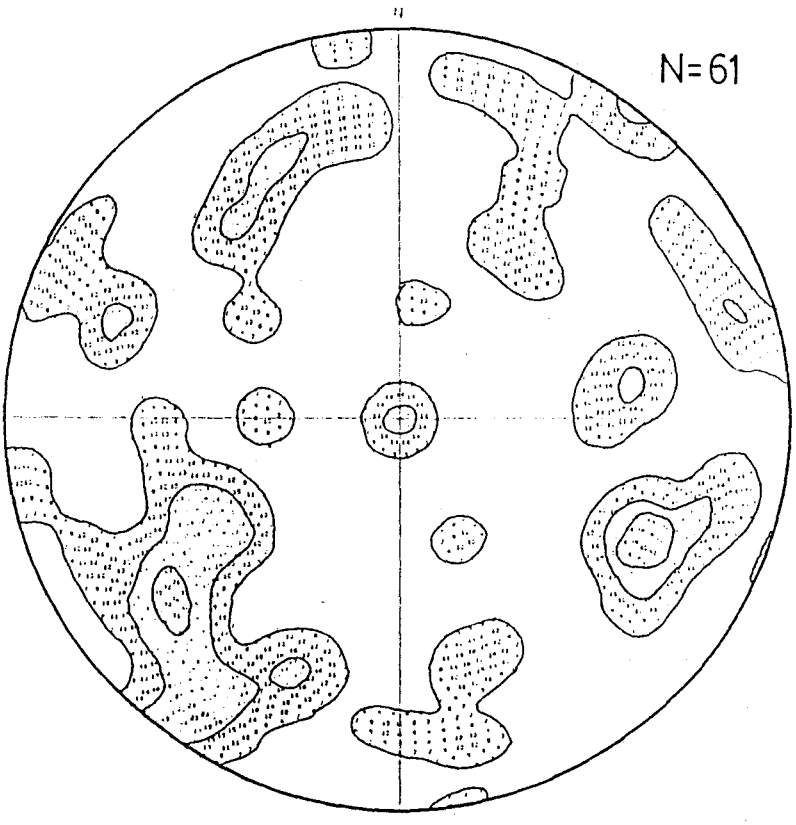

2a

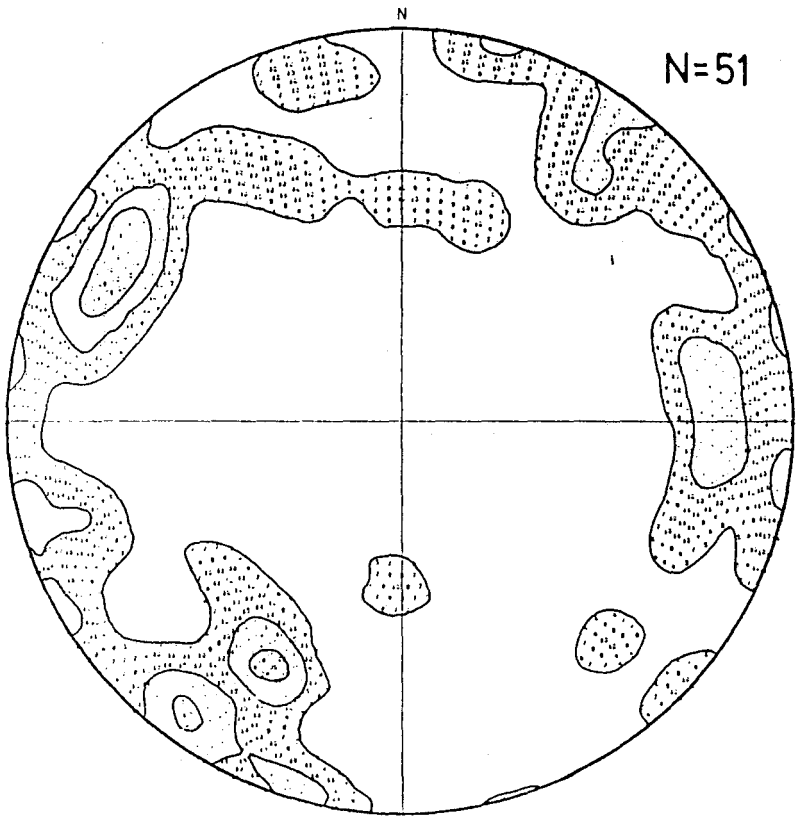

2b

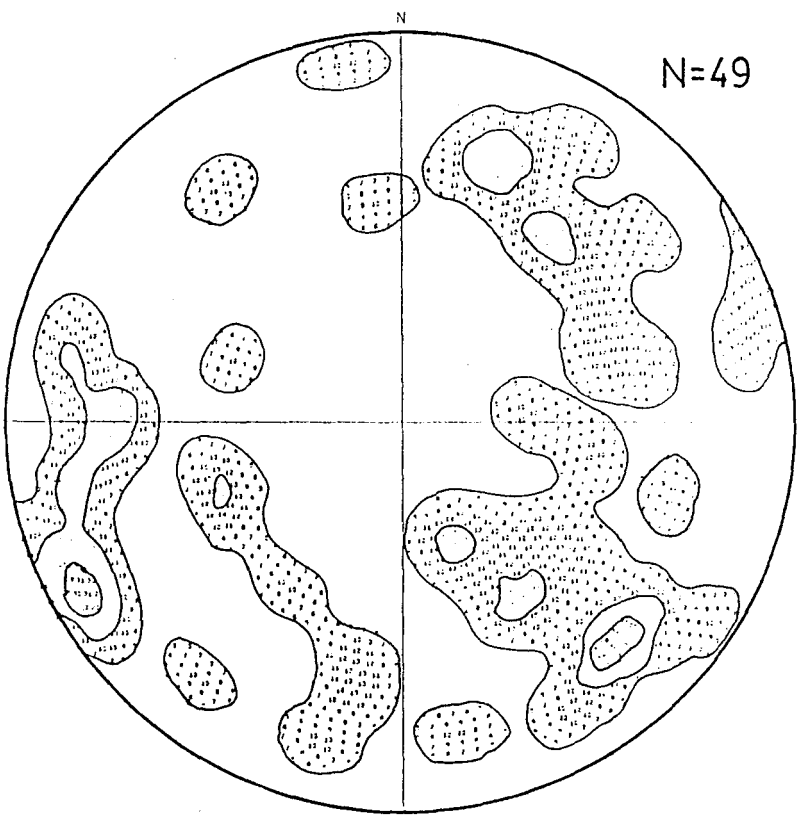

3a

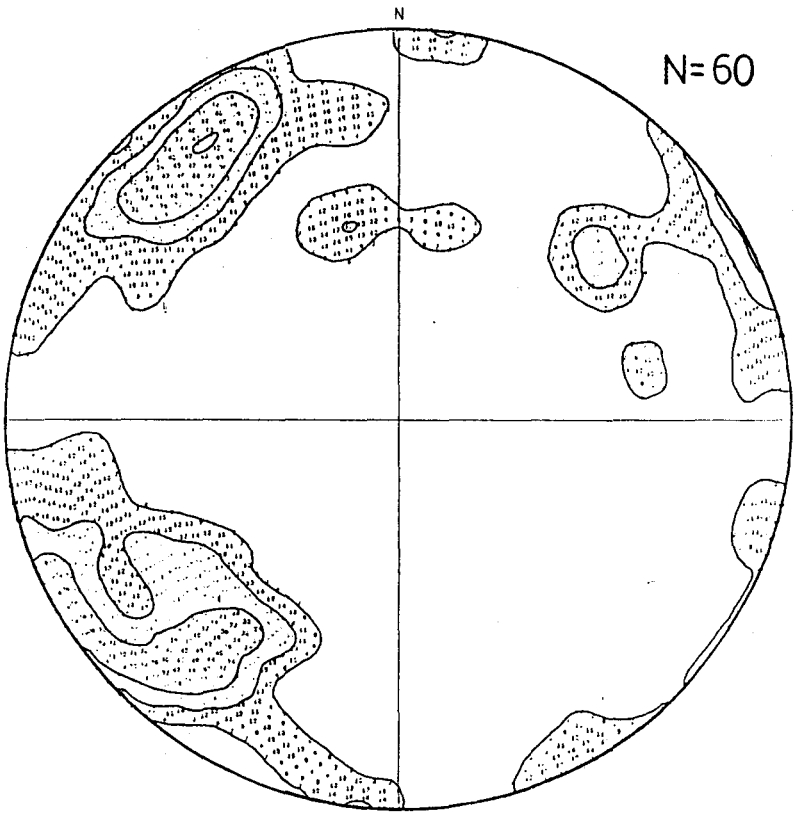

3b

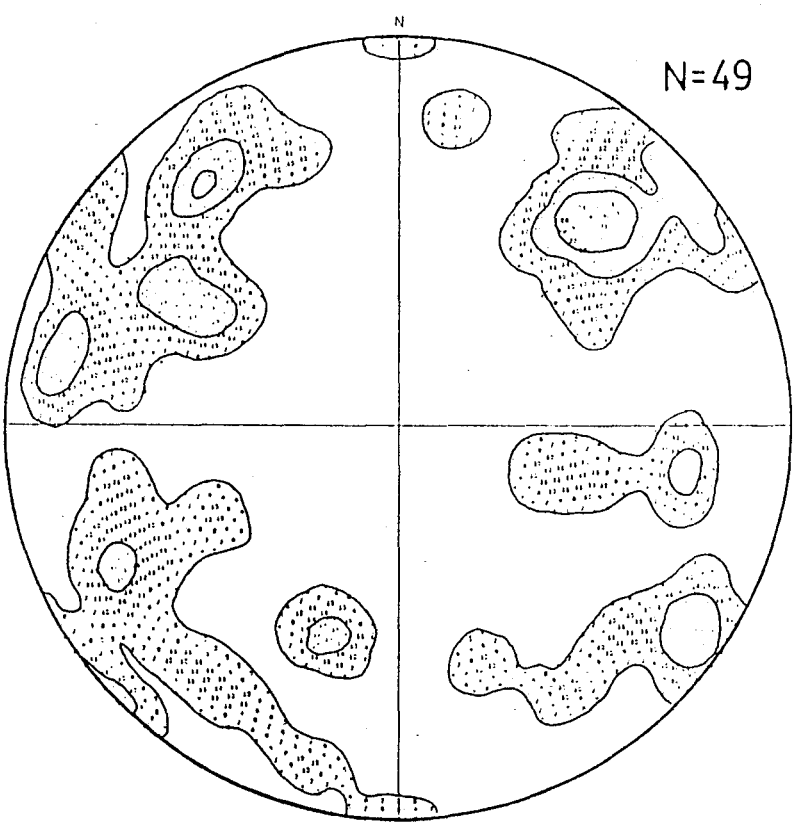

6a

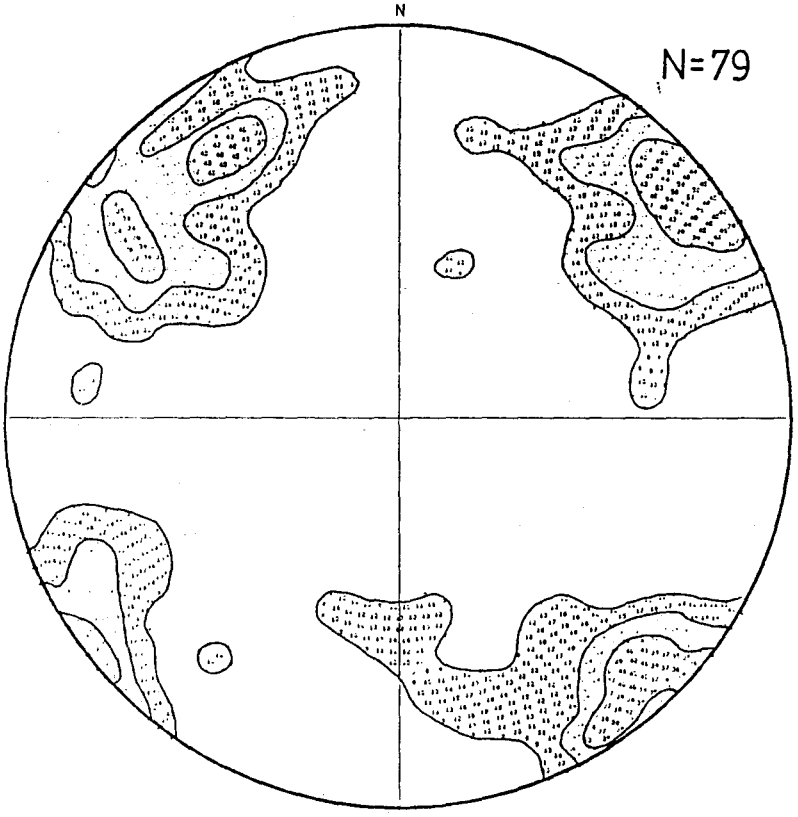

6b

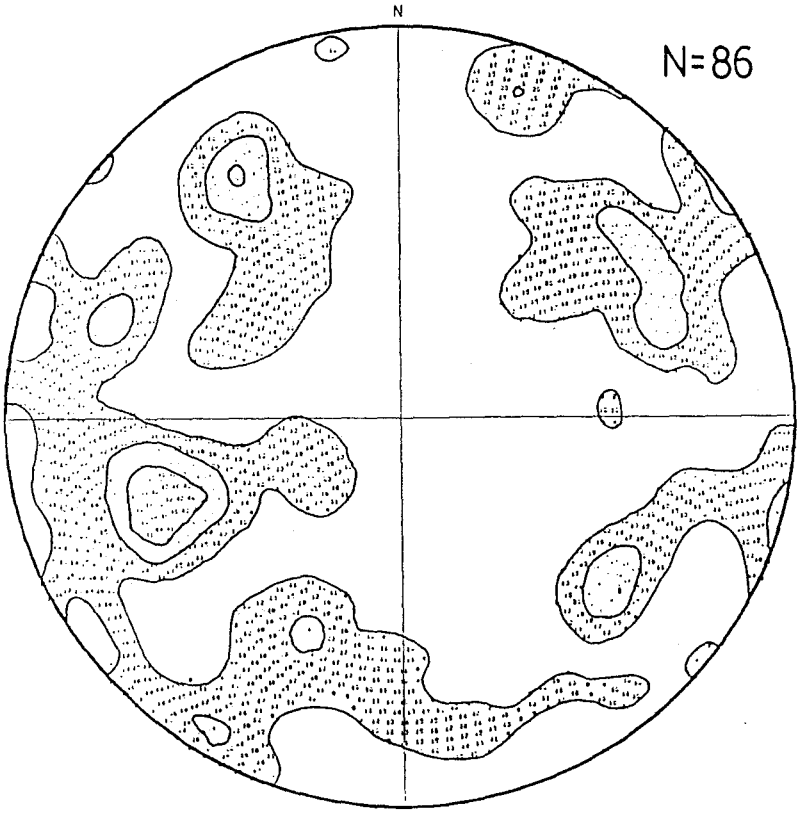

8a

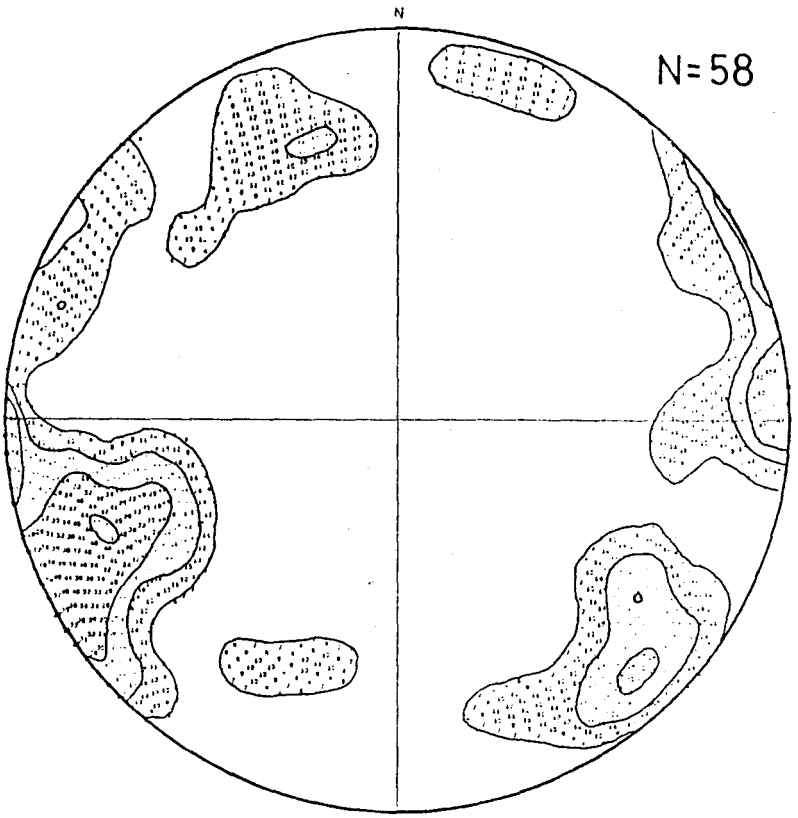

8b

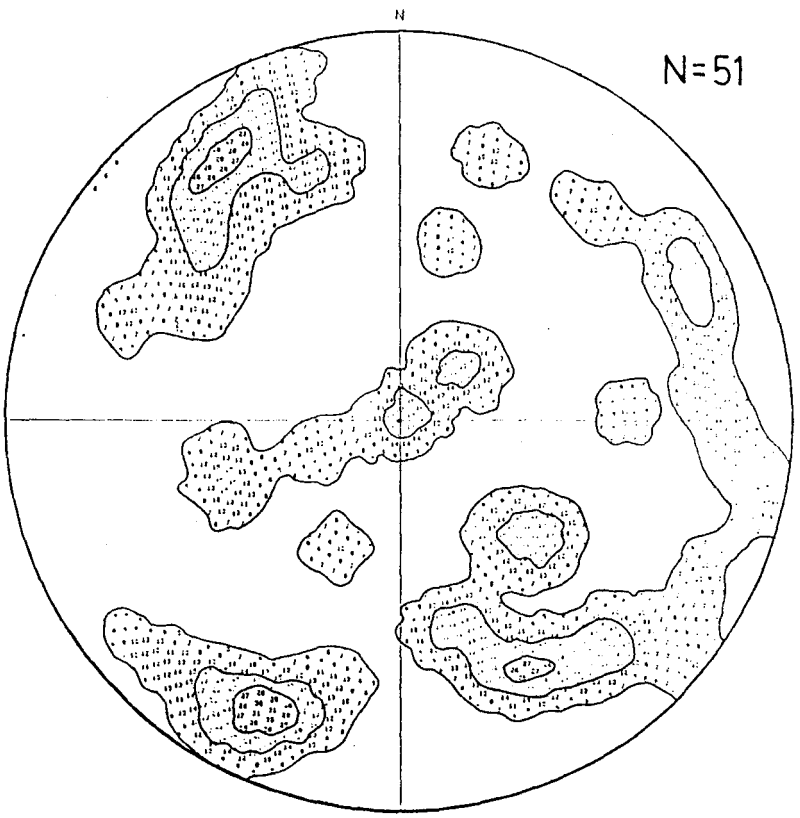

11a

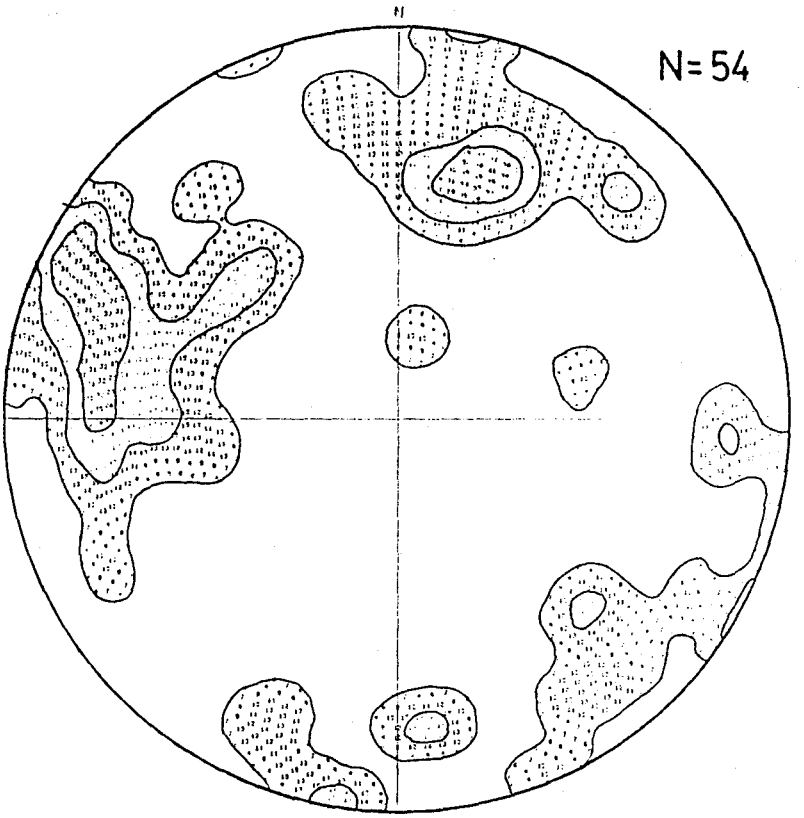

11b

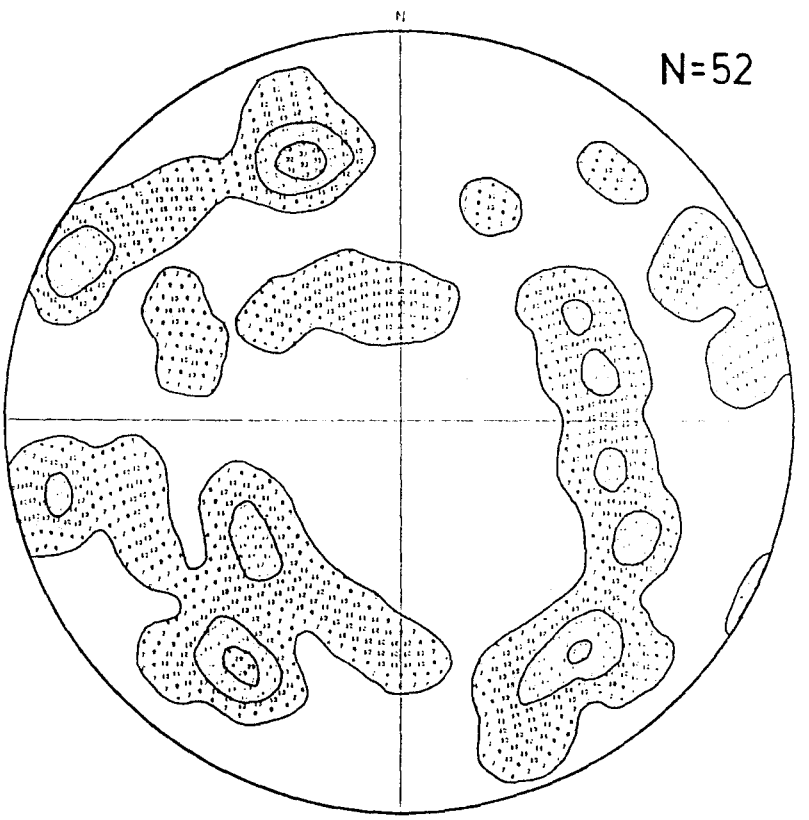

CHAPTER 3

Discussion and Interpretation

3.1 Histograms

Data from the histograms agree remarkably well with results from previous research. For example, 50% of the lamellae of Scott et al. (1965) lie in the 10^{o}-30^{o} interval while the mode of their data falls at 15^{o}-20^{o}. Results from the present study also compare well with those of Carter and Friedman (1965). They reported a mode of 20^{o}-25^{o} for 907 sets of lamellae in the Dry Creek anticline, while the majority of lamellae occupied the 10^{o}-45^{o} range. Hansen and Borg (1962), however, reported a significantly lower mode (10^{o}-15^{o}) for a similar study.

It is possible to relate the range of results above, as well as the results of this study, to the experimental findings of Carter, Christie and Griggs (1964). These showed the tendency of lamellae to fall in one of three categories; either at 0-20^{o}, 20^{o}-60^{o}, or subparallel to the C-axis. Perhaps the absence of more basal orientations in this study and in the studies of Carter and Friedman (1965) and Scott et al. (1965) is an indication of much lower strain rates associated with these types of deformations. In fact, the 3-dimensional phase diagram of Ave 'Lallemant and Carter (1971) would suggest this is so. It shows an increase in the volume of the subbasal field with decreasing strain rate. It should be remembered, however, that the right hand side of this diagram was

produced via extrapolation (see p. 231, Ave 'Lallemant and Carter, 1971), and so is merely postulation.

Whatever the case, Scott (1965, p. 733) mentions that slight differences in average orientation from one population of natural lamellae, and from populations of experimental to natural lamellae should be expected since not all can be assumed to have formed under the same environmental conditions, nor to have been produced by similar dynamic effects.

Unfortunately there is no basis for the comparison of the histograms of the present study with any of those displayed in Figure 6 (Ave'Lallemant and Carter, 1971). This is a necessary consequence of the assumption that the temperature and pressure accompanying this folding event were much lower than those used in the experiments of Ave'Lallemant and Carter (for further discussion of this assumption, see sections 3.2, 3.3). In fact, the most likely experimental analogues to this natural deformation are the squeezed samples produced at low temperature (approximately 200^{o} C) of Carter, Christie and Griggs (1964). However, the strain rates produced by the simple squeezer are much too high to be comparable to those assumed to have been operative during the creation of this fold. The consequence of the higher strain rates in the aforementioned experiments was the generation of dominantly basal lamellae. Presumably subbasal lamellae could be generated in similar experiments if the strain rate were lowered; this, of course, implies an increase in the

variable of time. Such a scenario seems reasonable for the production of lamellae in a fold whose formation occurs over a period of geologic time, the scale of which is orders of magnitude greater than the time scale of such experiments.

3.2 Estimate of temperature during folding

An estimate of the temperature during folding can be made through the use of conodonts. Harris (1979) has constructed conodont colour index maps for the Appalachian Basin for various geologic time periods. By assuming that sedimentation ceased in the basin somewhere in the interval Late Pennsylvanian (300 my) to Middle Triassic (235 my) it is possible to derive minimum and maximum temperature ranges associated with burial and heating. If we also assume that sedimentation was contemporaneous with deformation, which seems reasonable, we can estimate the approximate temperature which accompanied this folding event. Since the folding itself occurred in the time slot Late Devonian - Early Mississippian (Acadian orogeny), the temperature derived by assuming that sedimentation ceased in the Late Pennsylvanian will likely be the most accurate.

Fig. 15 is a conodont colour isograd map. The approximate region within which the fold is located is given by the rectangle. This lies between the isograds CCI = 3.0 and CCI = 4.0. The temperature range can now be obtained using the Arrhenius plot (Epstein et al. 1977) (see Fig. 16). The minimum time for burial is 100 my

Fig. 15 Conodont colour isograd map (Harris, 1979) for Silurian through Middle Devonian limestones in the Appalachian Basin. The fold of the present study is located within the region outlined by the rectangle (+ = approximate location).

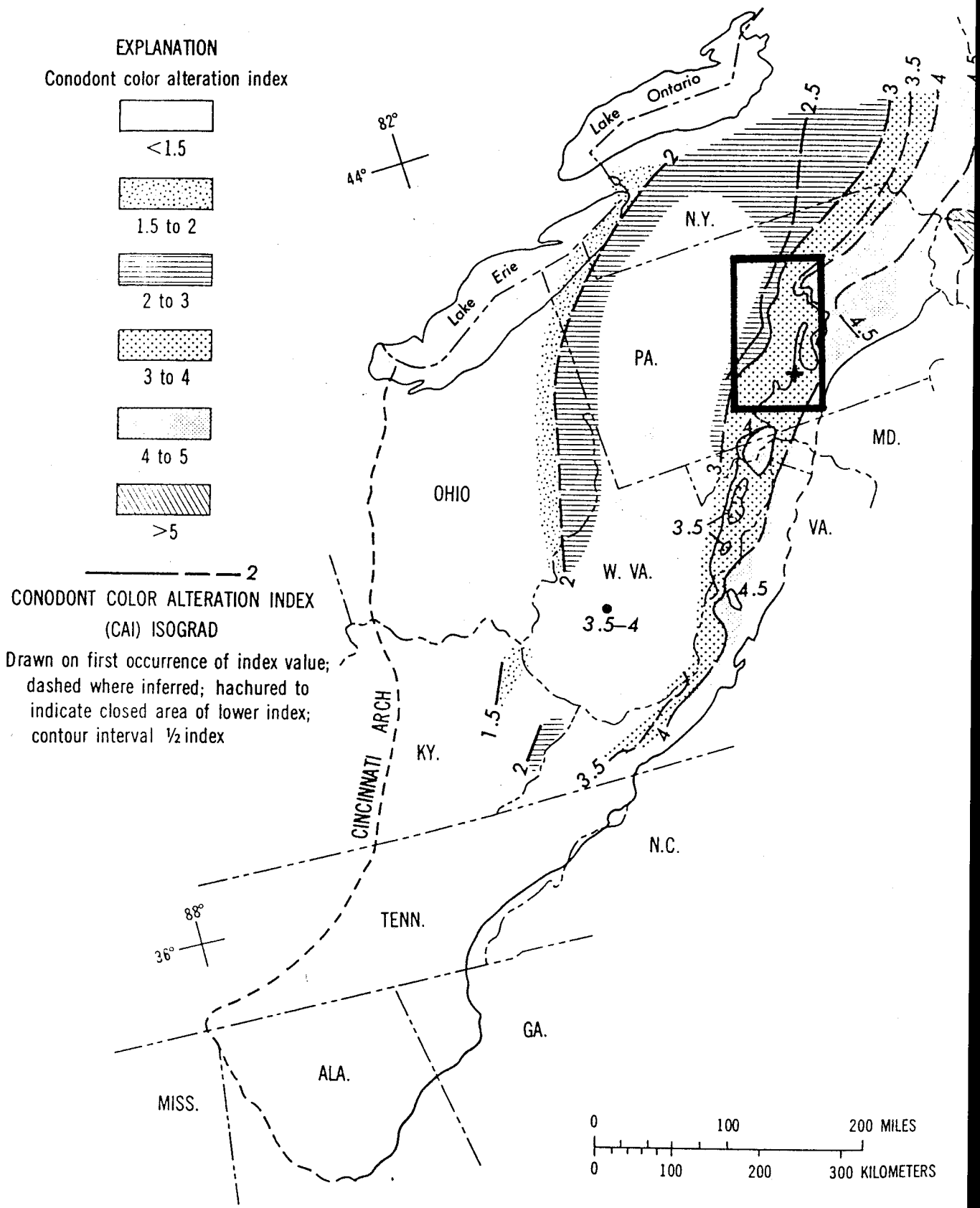
EXPLANATION
Conodont color alteration index
<1.5
1.5 to 2
2 to 3
3 to 4
4 to 5
>5
2
CONODONT COLOR ALTERATION INDEX (CAI) ISOGRAD
Drawn on first occurrence of index value; dashed where inferred; hachured to indicate closed area of lower index; contour interval ½ index
82°
44°
Lake Ontario
Lake Erie
N.Y.
PA.
OHIO
W. VA.
MD.
VA.
KY.
N.C.
TENN.
GA.
ALA.
MISS.
CINCINNATI ARCH
3.5–4
88°
36°
0 100 200 MILES
0 100 200 300 KILOMETERS

(Early Devonian (400 my) - Late Pennsylvanian (300 my)). The maximum time is 165 my (Early Devonian (400 my) - Middle Triassic (235 my)). These give an average temperature range from 115^{o}-190^{o} (see Fig. 16 for details).

3.3 Estimate of Pressure during folding

Assuming an average geothermal gradient the depth of burial for this temperature range would be from 5-10 km. However, this value is obtained assuming the stress field was hydrostatic which is, of course, not the case for a region under orogenic compression. If anything one would expect the geothermal gradient to increase in the presence of a non-hydrostatic stress field. The estimate of depth above can therefore be regarded as a maximum. In other words, it is more likely that folding of the Oriskany occurred with much less cover (2-3 kms?).

3.4 Regime of T, P, strain rate

On the basis of the above criteria, and with the additional assumption that the strain rate is in the range 10^{-12} to 10^{-14} sec^{-1} it is possible to give an approximate field in temperature, pressure, strain rate space for this deformation. The position of this field in the phase diagram of Ave'Lallemant and Carter (1971) is shown in Fig. 17. It falls in the "extrapolated" right hand region of the diagram. It is postulated that the subbasal I field extends to this portion. Results from the present study support such a claim.

Fig. 16 Arrhenius plot (Epstein et al., 1977).

The ordinate value, 130 my, represents an "average" as between maximum burial time (165 my) and minimum burial time (100 my). The corresponding average temperature range is derived by taking the temperatures at which the 130 my time line intersects CCI = 3.0 and CCI = 4.0. It is approximately 115^{o}-190^{o}.

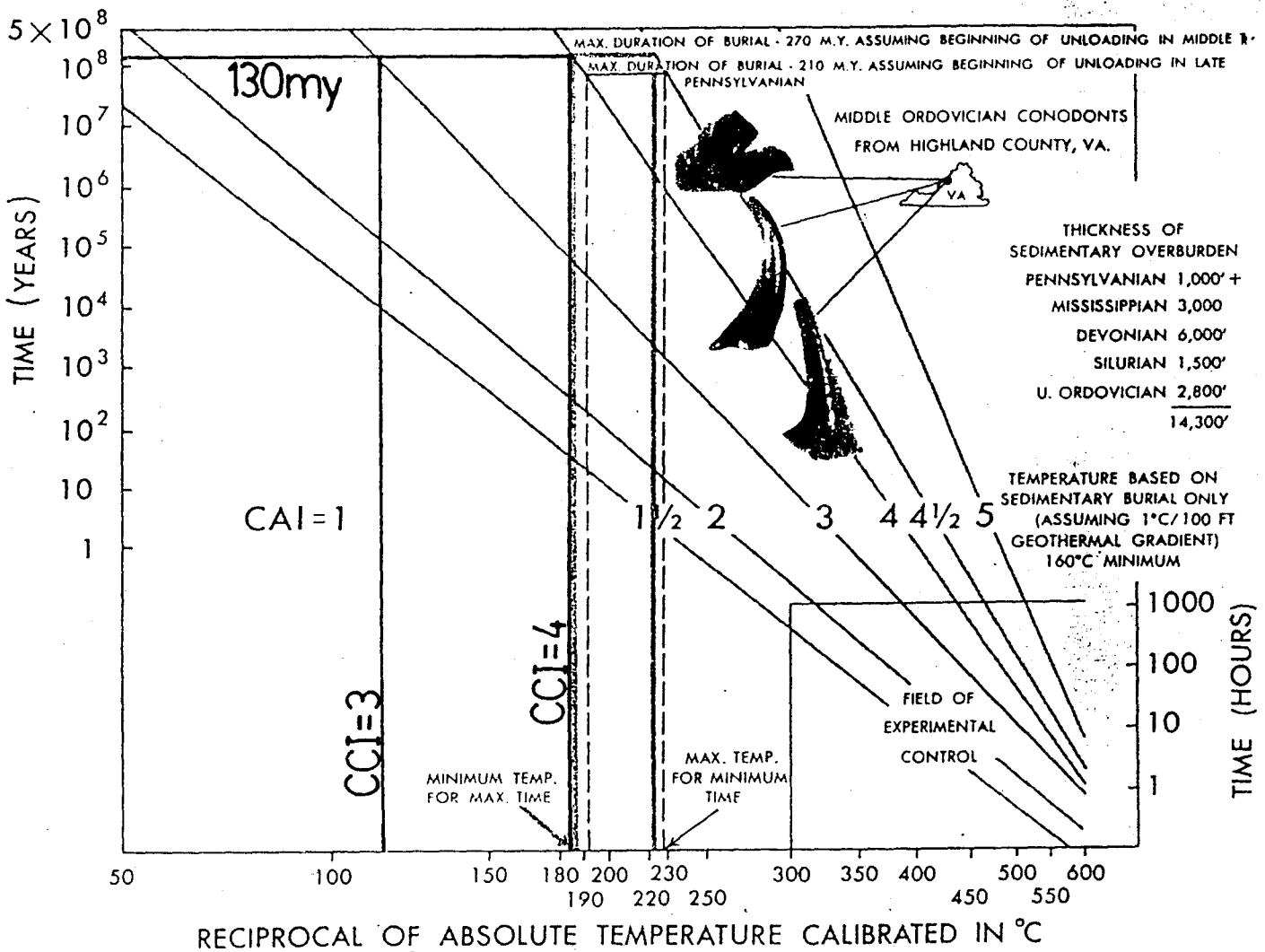
MAX. DURATION OF BURIAL - 270 M.Y. ASSUMING BEGINNING OF UNLOADING IN MIDDLE P
MAX. DURATION OF BURIAL - 210 M.Y. ASSUMING BEGINNING OF UNLOADING IN LATE PENNSYLVANIAN
130my
MIDDLE ORDOVICIAN CONODONTS FROM HIGHLAND COUNTY, VA.
VA
THICKNESS OF SEDIMENTARY OVERBURDEN
PENNSYLVANIAN 1,000'+
MISSISSIPPIAN 3,000
DEVONIAN 6,000'
SILURIAN 1,500'
U. ORDOVICIAN 2,800'
14,300'
TEMPERATURE BASED ON SEDIMENTARY BURIAL ONLY (ASSUMING 1°C/100 FT GEOTHERMAL GRADIENT) 160°C MINIMUM
TIME (YEARS)
5×10^8
10^8
10^7
10^6
10^5
10^4
10^3
10^2
10
1
CAI=1
1½ 2 3 4 4½ 5
CCI=3
CCI=4
FIELD OF EXPERIMENTAL CONTROL
MINIMUM TEMP. FOR MAX. TIME
MAX. TEMP. FOR MINIMUM TIME
1000
100
10
1
TIME (HOURS)
50 100 150 180 190 200 220 230 250 300 350 400 450 500 550 600
RECIPROCAL OF ABSOLUTE TEMPERATURE CALIBRATED IN °C

Fig. 17 Three-dimensional phase diagram showing various "mechanism" fields of lamellae formation in T, P, strain rate space (Ave'Lallemant and Carter, 1971). The stippled volume on the right hand side of the diagram shows an approximate field for the deformation process associated with the production of the fold of the present study.

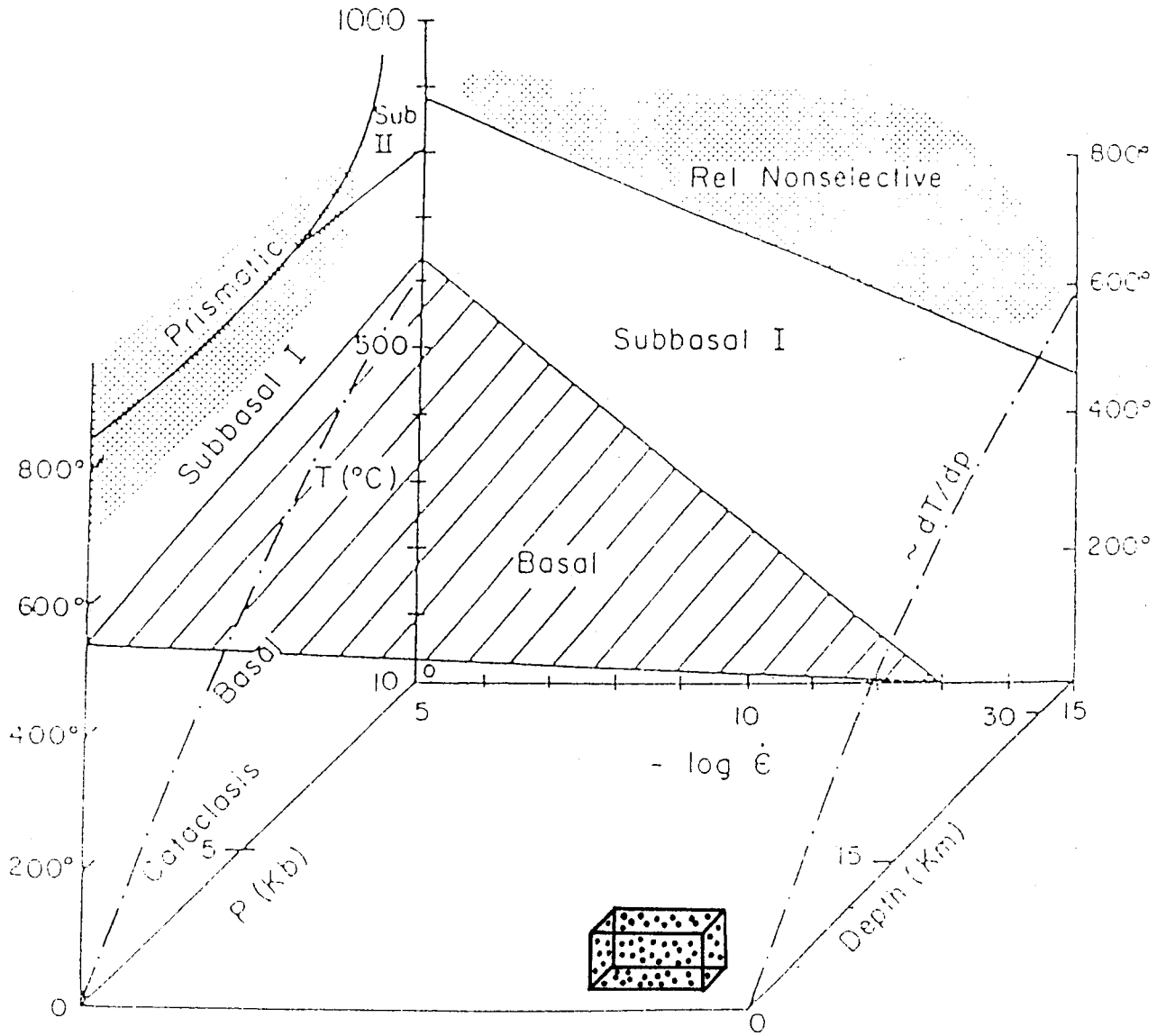
1000
Sub II
Prismatic
Rel Nonselective
800°
600°
400°
200°
Subbasal I
500
T (°C)
Subbasal I
Basal
~ dT/dp
Basal
10
0
5
10
30
15
- log $\dot{\epsilon}$
Cataclasis
5
P (Kb)
15
Depth (Km)
0
0

3.5 Significance of Additional Measurements

The generally random orientation of C-axes of grains without lamellae versus the non-random orientation of those with lamellae, and the lack of correspondence in fabric as between the two cases suggests that the lamellae are not artifacts of an original preferred orientation of quartz grains within the sandstone. This is an important observation, as it means that the fabrics of lamellae are true indicators of the stress field of the last dynamic event, rather than a manifestation of a pre-existing fabric in the rock. If the latter were true the lamellae would not serve as useful guides for stress orientations.

3.6 Stress Analysis

3.6.1 Previous Interpretation

Buhay (1985, p. 81) postulated that both a local, bedding parallel, and a regional component of stress acted on the folding layer. Based on more extensive fracturing in the hinge zone he presumed values of strain were higher there. This contrasted with evidence for less strain in the fold limbs. He attributed the higher strain to the bedding parallel and regional components coinciding in orientation in the hinge zone versus occurring at low angles to one another in the fold limbs. A schematic sketch of this situation is given in Figure 18. Intuitively this makes sense. It is also worth mentioning that some of the best deformation lamellae occurred at Station 5. It is

Fig. 18 Bedding parallel, and regional components of stress acting on the folded layer (Buhay, 1985).

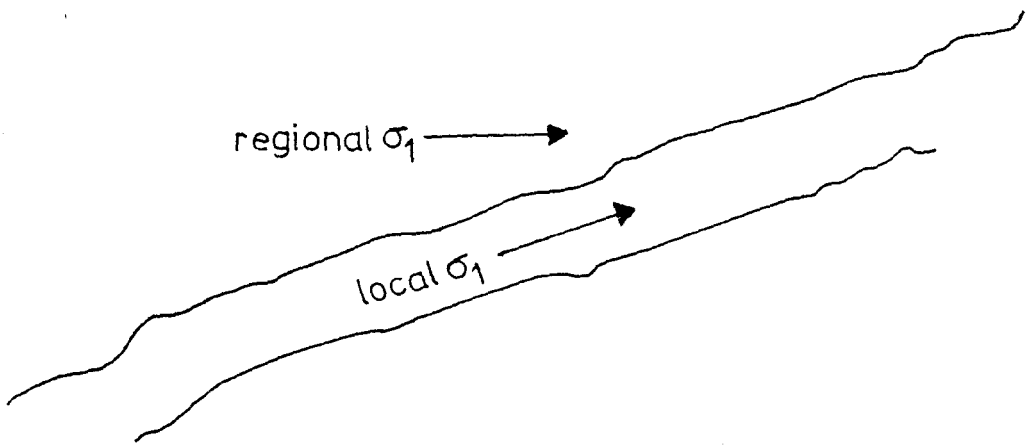
regional σ_1
local σ_1

here, as well, where a kink in the folded layer occurs. Perhaps this was a point of high directed stress during the evolution of the fold.

3.6.2 σ_i from Deformation lamellae

A common pattern for poles to deformation lamellae is two point maxima 90° apart (Fairbairn, 1941; Turner, 1948). This geometrical arrangement suggested to earlier workers that the lamellae had formed on planes of maximum resolved shear stress at an average of 45° to σ_1. Because such shear planes are oriented by convention at 45° to the greatest and least principal stresses (σ_1, σ_3) one can infer that the intermediate stress coincides with the line of their intersection. Thus the two "average" orientations of lamellae intersect at σ_2, and the bisectors of these two average orientations are parallel to either σ_1 or σ_3, as the case may be (see Scott et al., 1965, p. 741).

The average geometrical relationships of lamellae across this fold accord with this hypothesis. Poles to lamellae generally show four maxima which are arranged in a consistent fashion from one station to another (see Fig. 13(a), (b)). Angles between maxima are not 90°, however. Instead we find that the average angle between maxima in the upper quadrants is 60°-70° (acute bisectrix) while that between maxima in opposing halves of the diagram is 110°-120° (obtuse bisectrix). In addition, maxima can be joined along small circle girdles (complete or incomplete) of three basic types (see section 2.3.2, Fig. 13(a), (b)).

Presumably the conical surfaces defined by these girdles in 3-D are also surfaces of high shear stress (Christie and Raleigh, 1959, pg 399).

Given the assumption that σ_2 occurs at the intersection of the two mean orientations of lamellae, in the plane of bedding, it follows that either of σ_1 or σ_3 lie along the bisectors of the acute and/or obtuse angles between these orientations (see Fig. 19(a)). This would suggest that either of σ_1 or σ_3 is roughly bedding parallel, or alternatively, that it is bedding perpendicular. If the deformation lamellae formed in response to the regional compression associated with folding, one would expect the former condition to hold i.e. σ_1 bedding parallel. However, if the lamellae formed due to a vertical, compressive event unrelated to folding one would expect the latter arrangement i.e. σ_1 bedding perpendicular.

The typical arrangement of small circle girdles supports the suggested positions for stresses above. For example, at almost all stations an incomplete small circle girdle of radius 70^{o} was defined in the plane of the diagram. The axis of the cone defined by this girdle corresponds to the proposed direction of σ_2. A similar relationship exists for cones defined by small circle girdles about the north or south of the diagrams. Here either of σ_1 or σ_3 is parallel to the cone axis. Such a direction is similar to that given by the bisector of the acute angle between average orientations of lamellae (see Fig. 19(a), (b)).

Fig. 19 (a, b) Stress directions given by "average" lamellae orientations. (c) Stress directions given by "average" C-axis orientations.

σ_i , σ_j = σ_1 , σ_3

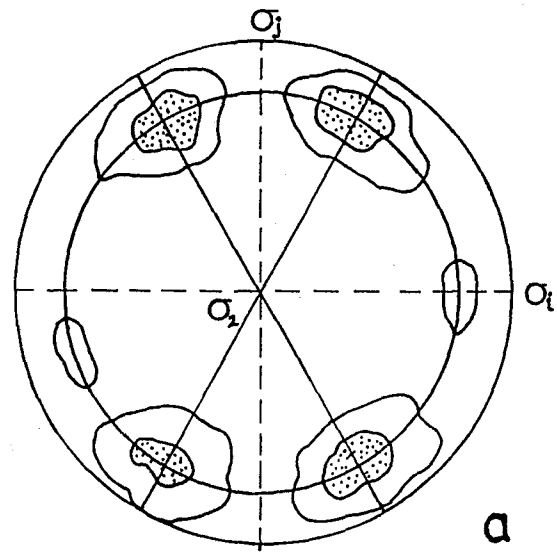

a

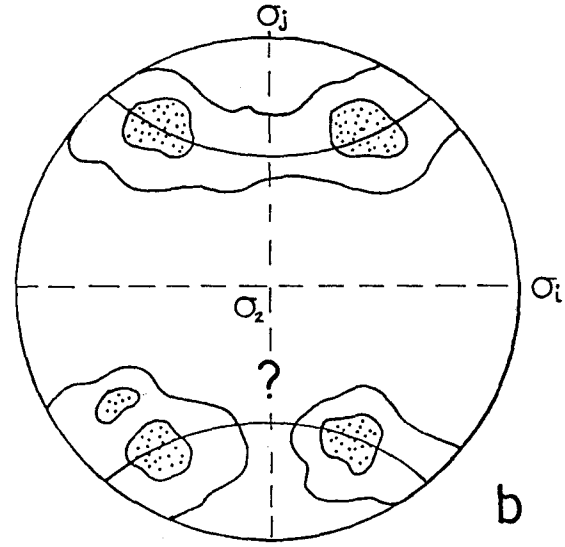

b

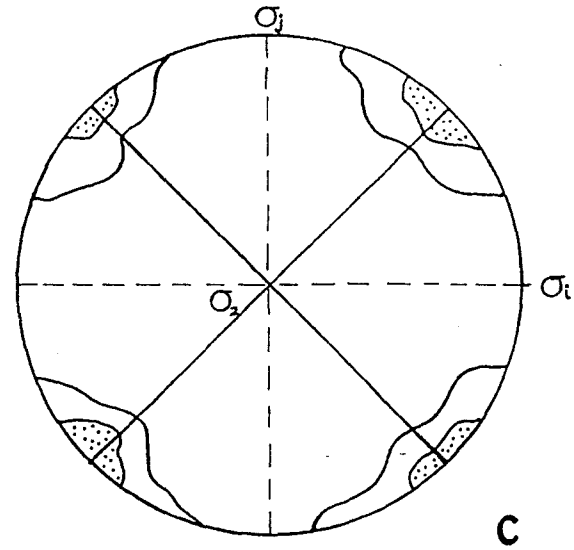

c

3.6.3 σ_i from C-axis

The C-axis fabrics suggest a similar arrangement for stresses as do poles to quartz lamellae (see Fig. 19(c)). σ_2 is most likely located at the intersection of lines joining maximas in opposite quadrants and either of σ_1 or σ_3 is bedding parallel or bedding perpendicular, as the case may be.

3.6.4 σ_i from Arrow Diagrams

Section 1.4 (p. 13-14) of the introduction discussed application of the arrow method in stress analysis. Arrows joining C-axis and pole to quartz lamellae point towards σ_3 (for $\sigma_3 < \sigma_1 = \sigma_2$), towards a great circle containing σ_2 and σ_3 (for $\sigma_1 > \sigma_2 = \sigma_3$), or contain σ_1 and σ_3 ($\sigma_1 > \sigma_2 > \sigma_3$) with the arrow head always positioned closest to σ_3 (as modified from Carter and Raleigh, 1969).

Mutually perpendicular lines x and y were drawn on the arrow diagrams to display symmetrical groupings of arrow trends (see Fig. 12, p. 31-41) x and y can now be taken as equivalent to stress directions since in each case they are bisectors of the mean orientations of both lamellae and C-axes. Their intersection therefore defines the position of σ_2 and they themselves define the positions of σ_1 and σ_3.

To determine which of x or y is σ_1 or σ_3 one must examine trends of arrow direction. These trends are summarized on p. 42. The most obvious for which to account is a tendency for arrows to point away from bedding

towards the north or south of the diagram respectively. Another trend to consider is one in which the arrows point from the outer edge to the inner region of the diagram. These trends suggest two possibilities. The first is that σ_3 is subparallel to the north-south direction of the diagram, and that the condition $\sigma_2 = \sigma_1 > \sigma_3$ holds. The second is that $\sigma_1 > \sigma_2 = \sigma_3$ as is implied by arrows pointing towards the great circle containing σ_2 and σ_3, which is located in the "inner" region of the plot, roughly coincident with its north-south diameter. Perhaps it is possible to have a combination of these two conditions. Such a combination might indicate a change in the stress field over the duration of folding where σ_2 is seen to alternate between being nearly equivalent to σ_1 on one hand and to σ_3 on the other. Thus the amount of compression parallel to the fold axis might have varied through time. Whatever the case, the data are good enough to suggest, at the very least, that $\sigma_1 > \sigma_3$ for this fold. In addition, it supports a stress geometry where σ_1 is bedding parallel and σ_3 is bedding perpendicular, with σ_2 occurring at their intersection.

As explained earlier, lines x and y are offset in a clockwise or counterclockwise direction from the north-south or east-west directions of the diagram in a systematic fashion across the fold. Hence, σ_1 deviates from being parallel at some stations (6, 1) to occurring at low angles to bedding (15^{o}) at others (2, 3, 5, 8 and 11).

Figure 20 displays the stress orientations at each

station around the fold. At each station, σ_2 is assumed to occur at the intersection of σ_1 and σ_3, in a direction perpendicular to the plane of the paper.

3.7 Timing of Lamellae Formation; Dynamic Analysis

Lamellae appear to have formed prior to, or just at the onset of, crystallization of the secondary quartz cement. The fractures studied by Buhay (1985) clearly post-date both the deformation lamellae and cement. This is well documented in thin section where fractures commonly penetrate grains that have otherwise continuous sets of lamellae on either side of them (see Fig. 21). The cement is also disrupted by such fractures. In places these cross the thin section over distances of several centimenters.

Presumably the fractures were generated during bending or incipient bending when the stress experienced by the rock was such that it was reaching its critical strength. By this point it is assumed that lamellae would have formed already, and that their fabrics would have been "frozen" into the rock. It is difficult, if not impossible, however, to judge exactly when the lamellae enter the fold's dynamic history. Three possibilities present themselves. The first is that lamellae were generated after folding. This can be eliminated on the basis of the criteria above; that is, lamellae clearly pre-date the fractures, which themselves are assumed to have been created in the later stages of the folding process. The remaining two are given below:

Fig. 20 Stress orientations across the fold. Arrows give the direction of the maximum principal stress, σ_1. σ_2 occurs at the intersection of σ_1 and σ_3 at each station.

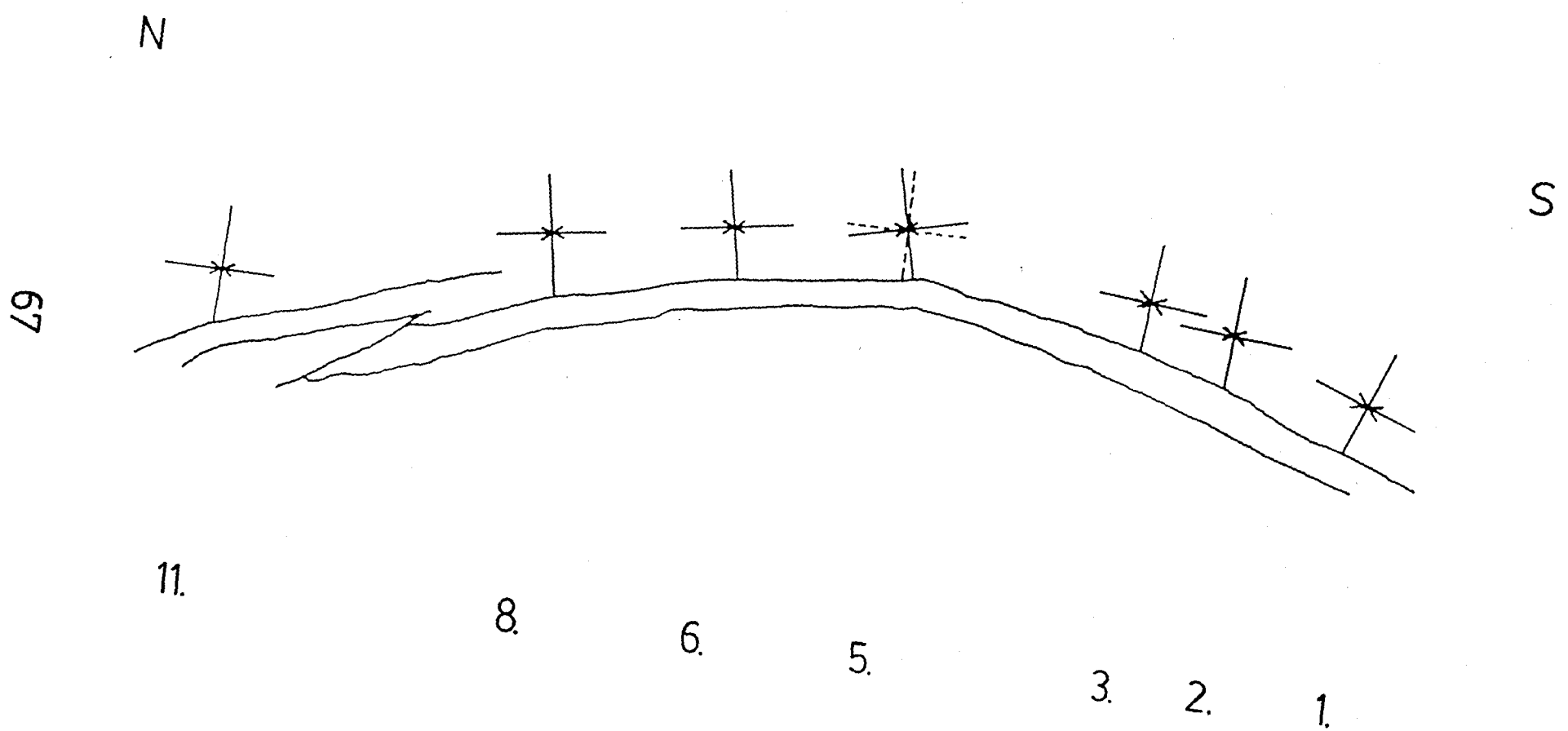
N
S
67
11.
8.
6.
5.
3.
2.
1.

Fig. 21 Sketch showing microfractures which cross-cut deformation lamellae.

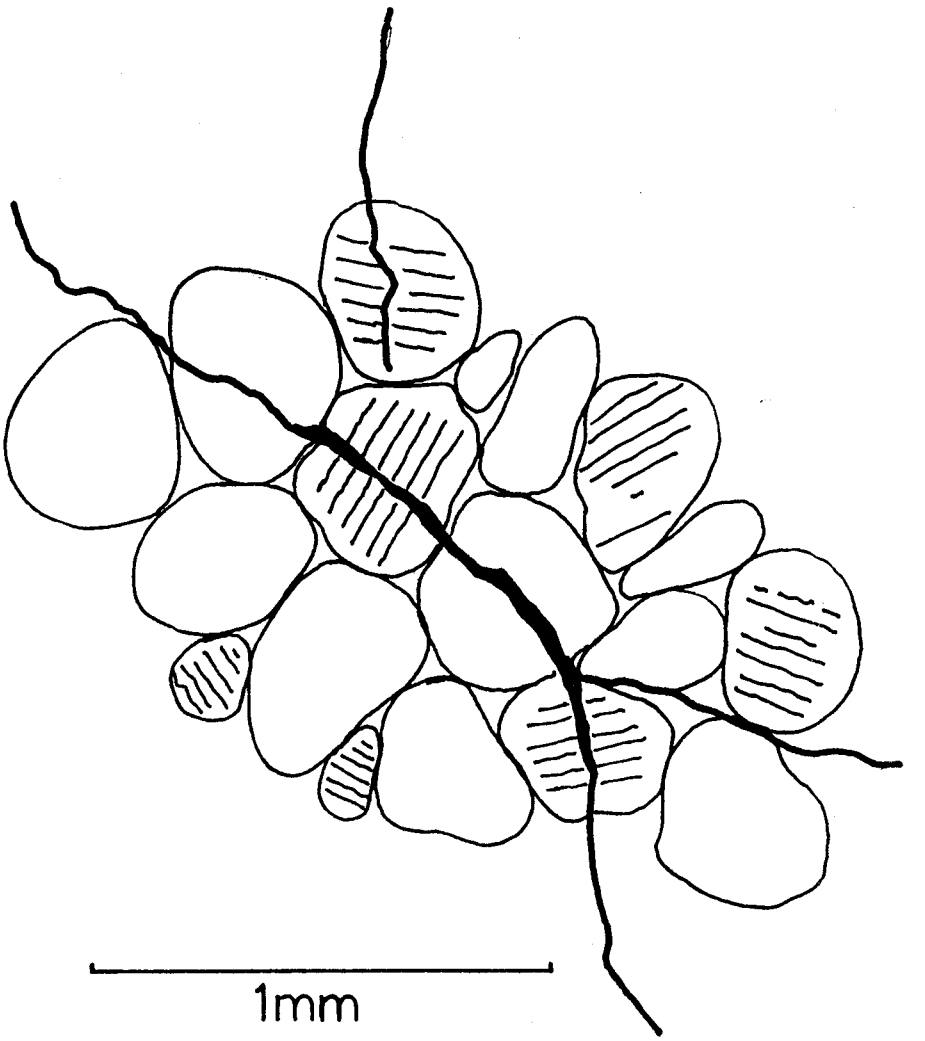
1mm

1. Lamellae formed due to orogenic compression when the bed was flat lying i.e. restored to original topography.

2. Lamellae formed after bending began. Judging from the geometry of the stresses across the fold this would require stress refraction, particularly on the fold limbs, by angles of less than 20^{o}. Such a situation is entirely plausible.

Discussion

1. Fig. 22(a) shows the present day configuration of stresses across the fold. Below it, (Fig. 22(b)), the bed has been unrolled, and is flat lying. The approximate change in orientations of stresses after unrolling are indicated. None are consistent with a direction of compression which is horizontal, or bedding parallel. In order to bring the maximum principal stress coincident with the horizontal at every station it is necessary to bend the layer so as to arrive at the geometry depicted in Fig. 22(c). This geometry might represent the original topography upon which a horizontal north-south compression would have had to act in order to generate the lamellae fabrics now retained in the folded rock. Note that two versions ((c), (d)) are given in accordance with the two interpretations of stress directions at Station 5.

2. On the other hand, it is entirely possible that bending had started before the onset of lamellae formation. As Buhay (1985) suggested, the phenomenon of stress refraction may have been prevalent in the fold limbs, while at the hinge less refraction may have occurred. The present day configuration of stresses, without regard to the portion of

Fig. 22 (a) present day configuration of stresses across the fold. (b) approximate orientations of stresses when bed is "unrolled". (c, d) geometry of folded layer required to satisfy the assumption that σ_1 was horizontal upon initiation of deformation. (c) is constructed assuming a present day bedding parallel orientation of σ_1 at Station 5 (dashed arrows). (d) is constructed assuming a present day non-bedding parallel orientation of σ_1 (solid arrows).

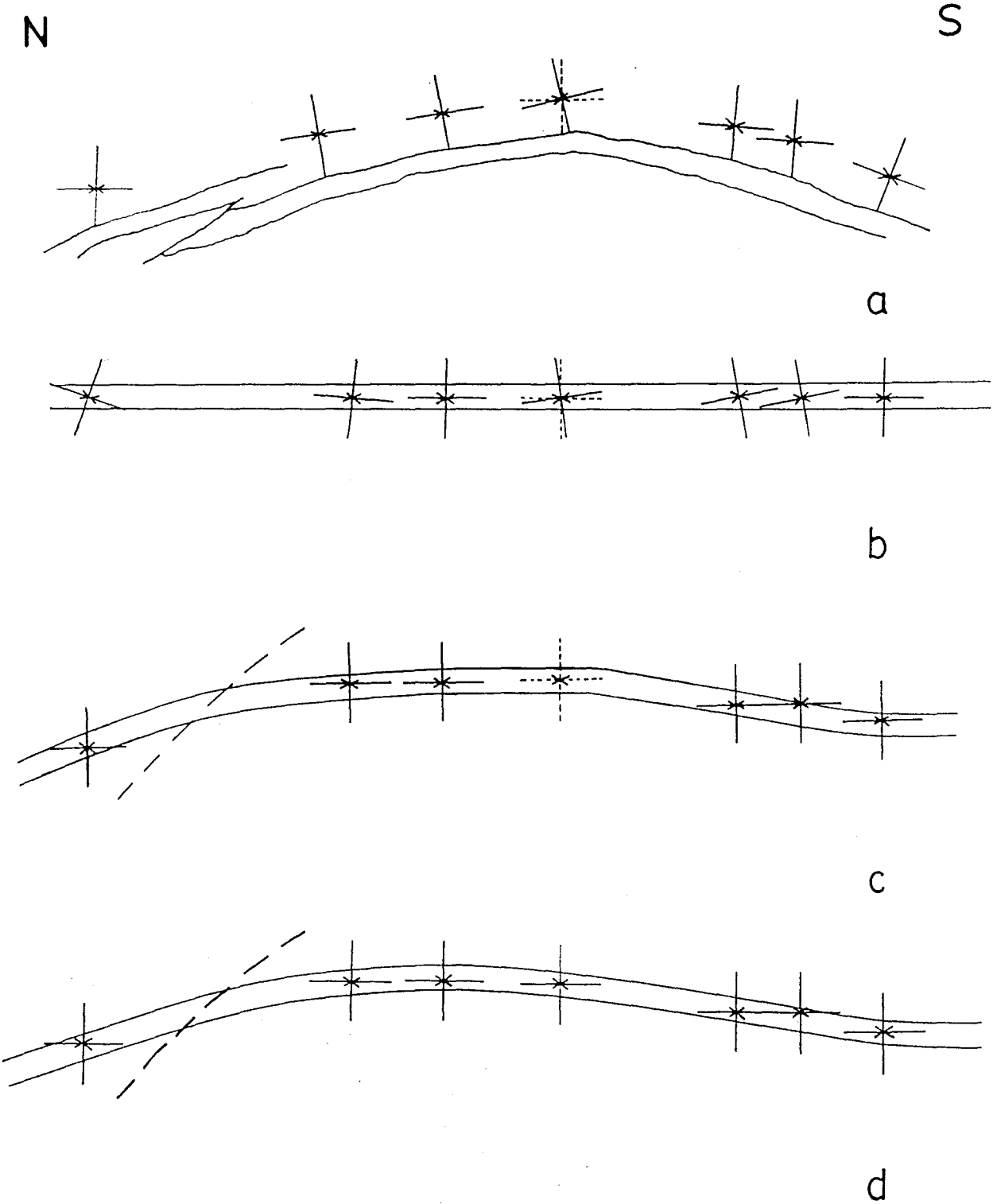
N
S
a
b
c
d

the fold to the north of the fault, supports this hypothesis quite readily.

The south limb of the fold, which has a more pronounced dip than the north limb, shows slightly higher angles of refraction compared to those of the latter. The fold hinge, roughly coincident with Station 5, has somewhat anomalous deformation lamellae fabrics; these may be indicative of stress refraction similar in amount and orientations to Stations 6 and 8 (solid arrows Fig. 20), or conversely, no refraction at all (dashed arrows). Whatever the case, it does appear that the rock at Station 5 deformed as the contiguous unit with the rock at Stations 6 and 8. Thus, the fold itself can be divided on the basis of general stress geometry by the kink in the bed just to the right of Station 5. On the north limb refraction occurs in a counterclockwise direction with respect to a regional horizontal stress, while on the south limb refraction takes place in a clockwise direction. The "kink" may have acted as a "pivot" position for bending.

The fabrics at Station 11 suggest that refraction did not occur, if it is assumed that the regional stress is horizontal. An explanation for this might be that upon movement along the fault, a once bedding parallel stress to the north of the fault was rotated in a clockwise fashion due to the release of pressure associated with failure. Alternatively this could be viewed as a "disequilibrium" of stresses on either side of the fault, resulting in rotation of the stress field on one (or both?) sides.

Either of 1 or 2 above are conceivable for the timing of lamellae formation. Of interest to both is a theoretical model for stress trajectories developed by Carter and Dietrich (1969) for two-dimensional large amplitude folding of a viscous layer in a less viscous matrix. Sets of trajectories were determined for different fold types using a mathematical approach which involved modelling with velocity fields. Figure 23(a) shows the trajectories of σ_1 after 40% shortening in a layer regarded as representative of most natural folds (μ_1/μ_2 (viscosity contrast) = 42, L/h(aspect ratio) = 12, A_o (initial amplitude) = 0.1 h). The second diagram (Fig. 23(b)) shows the variation in total strain across the folded layer. Curves of % shortening versus stress for various localities within the fold (see inset) are given. As is evident, the middle area of the limbs (cell 29) experiences high compressive stress during initial stages of folding. As folding progresses the magnitude of the stress decreases and the angle between σ_1 and bedding increases. At the nose of the fold, two trends are visible. Along the inner arc σ_1 is initially bedding parallel and remains so during the course of fold development. This zone also experiences the most compressive stress, both during initial stages and for the remainder of folding. Stress development along the outer arc sees σ_1 start out as bedding parallel and later rotate so as to become bedding perpendicular. During this

Fig. 23 Theoretical stress history of folding a viscous layer in a less viscous matrix (Dietrich and Carter, 1969). Parameters used (μ_1/μ_2 (viscosity contrast) = 42, L/h (aspect ratio) = 12, A_o (initial amplitude) = 0.1 h) are representative of most natural folds.

(a) Orientations of σ_1 after 40% shortening

(b) Stress versus strain curves for various zones within the fold (see insert).

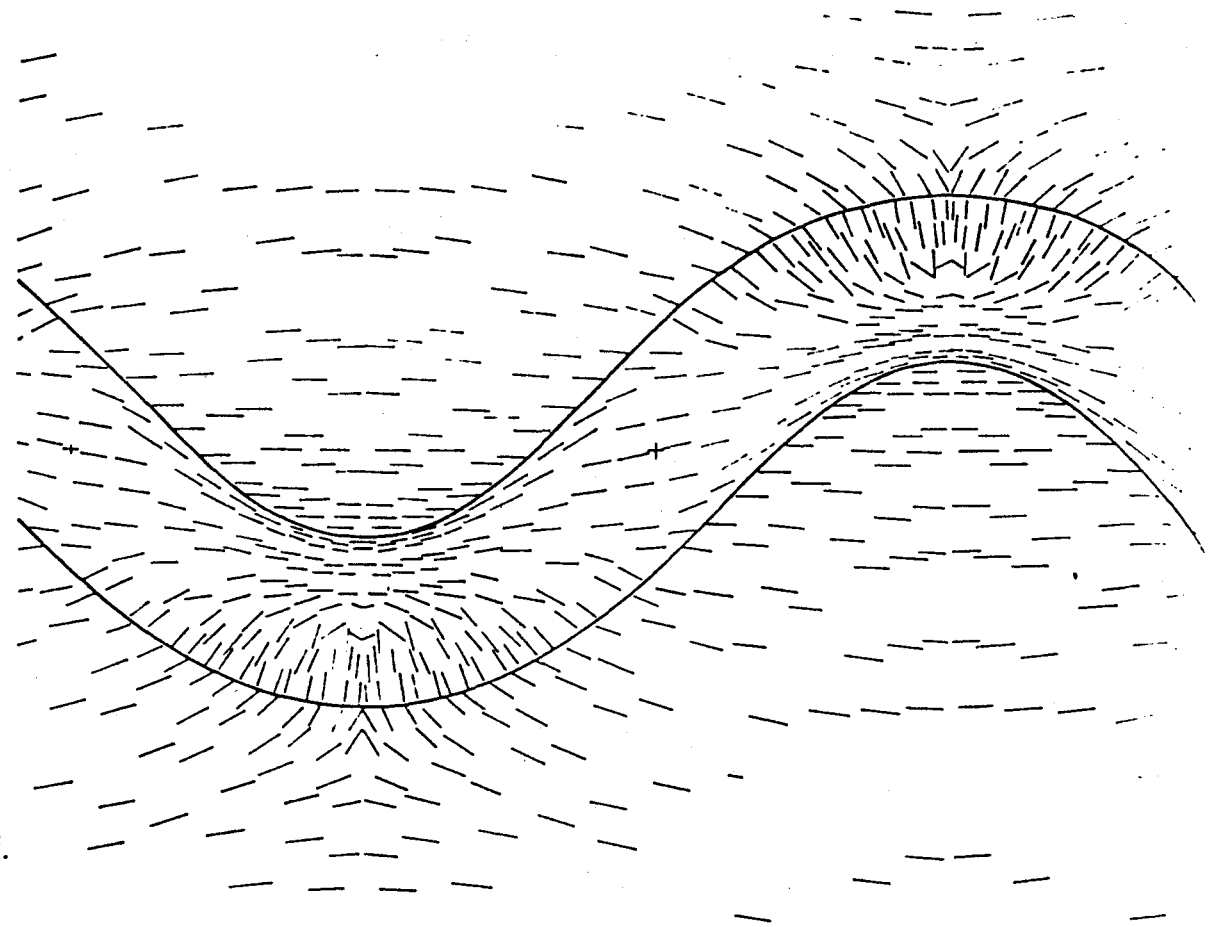

a.

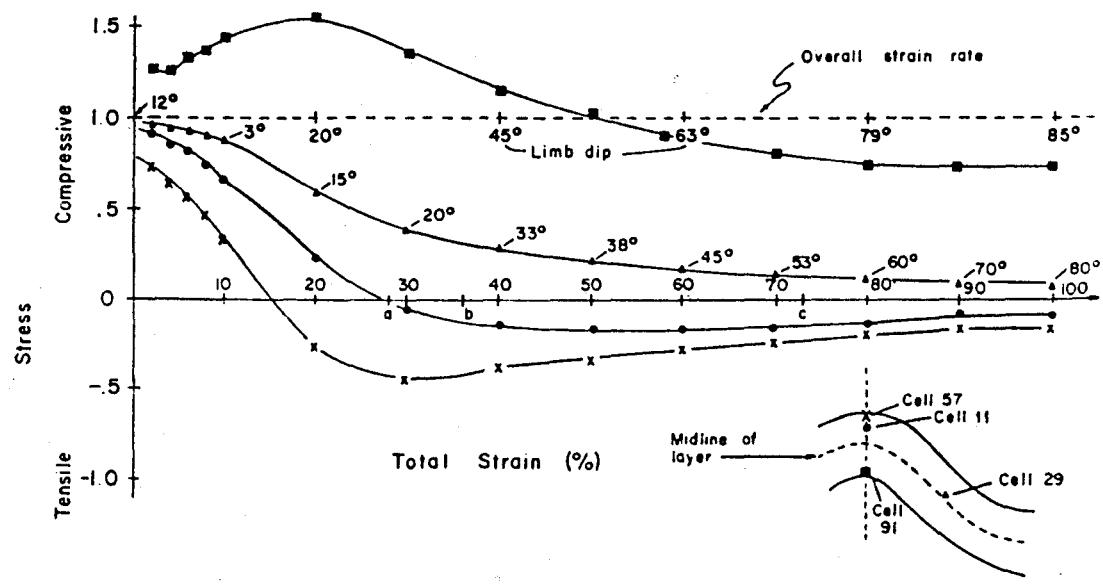
1.5
1.0
.5
0
-.5
-1.0
Compressive
Stress
Tensile
Overall strain rate
12°
3°
20°
45°
Limb dip
63°
79°
85°
15°
20°
33°
38°
45°
53°
60°
70°
80°
80°
90
100
10
20
30
40
50
60
70
a
b
c
Total Strain (%)
Midline of layer
Cell 57
Cell 11
Cell 29
Cell 91

b.

progression the stress regime changes from compressive to tensile in this zone.

According to Carter and Dietrich (1969, p. 150) most studies of natural folds, including those of Scott et al. (1965) and Carter and Friedman (1965), give conclusions consistent with this model. The model predicts, for example, that the greatest overall compression will occur in the interval of 0-10% shortening when σ_1 is inclined at low angles to bedding, or is bedding parallel. Thus, the most "probable" time for lamellae formation is during the early stages of folding, and the lamellae fabrics so generated imply a stress field with maximum compression parallel to the layer.

Data from the fold under study are also consistent with this model. However, it is still unclear at exactly what degree of bending, if bending at all, accompanied lamellae formation. In other words, were lamellae formed with virtually no stress refraction operative, or did they form with a small degree of stress refraction across the initially inclined limbs of the fold? One pertinent question to be raised in searching for a solution to this problem is how the original bedform might have accomodated a value of 0-10% shortening. Such an answer can only be derived from an extensive knowledge of the rheological properties of the rock and, of course, the original geometry of the layer.

Whatever the answers, it is clear that no definitive statement can be made as to which of options 1 or 2 for the

timing of lamellae formation applies to this fold. However, in light of the model of Carter and Dietrich (1969) it can be concluded that both are possible. Perhaps if this fold had developed a larger amplitude one might have been able to interpret from it a similar dynamic history to that of the fold studied by Scott et al. (1965). As it is, the lamellae fabrics in the present fold do not seem to have "passively" rotated very far with reference to what might have been their original attitude.

A further contribution the model possibly can make is to give an idea of the position of the bed studied with respect to the regimes of compression and tension of the folded unit as a whole (i.e. the whole Oriskany): that is, whether the bed is in the upper (outer arc), middle, or lower portion (inner arc) of the folded unit. Alternatively, the bed itself may have preserved a record of such stress regimes on a smaller scale.

Since σ_1 appears to have remained bedding parallel in the hinge area of the bed under study, and higher strain has apparently been accomodated in this region (see Section 3.6.1, p. 59), the model predicts that the bed lies somewhere below the neutral surface of the fold, where the hinge area remains in a compressional regime during folding. One problem with this prediction is that the stress orientations are derived from lamellae fabrics. These, in turn, may have formed early with respect to the deformation process as a whole. If the stress regime

evolved so as to become tensional in the outer arc of the hinge zone during a later stage of folding, then such a change would not be preserved by these lamellae fabrics. They would have already been frozen into the rock, during the earlier, generally compressional stage. Such may be the case for this fold. Buhay (1985) has documented a neutral surface within the bed itself, implying co-existing compressional and tensional regimes during fold evolution. However, his method of documentation, via orientations of microfractures, records an entirely different dynamic process from that associated with lamellae formation. It represents the very late stages of deformation when tensional processes dominate in outer arcs, not the very early stages.

A question of interest also is whether each bed in the folded unit (Oriskany as a whole) retains traces of its own dynamic development i.e. a neutral surface separating compressional (inner arc) versus compressional (outer arc) regimes, or whether the bed can be regarded as deforming homogeneously with beds above and below it, suggesting a larger scale stress regime to have been operative. Results of Buhay imply the former is true.

CHAPTER 4

Conclusions

Fabrics of deformation lamellae are useful determinants of paleostress directions. Geometrical relationships between lamellae and C-axis can also give an idea of temperature, pressure and strain rate required for lamellae formation, and hence can characterize more fully the nature of a deformation process.

For this fold, lamellae fabrics determine a stress field which had the arrangement; σ_1 bedding parallel, σ_3 bedding perpendicular, and σ_2 fold axis subparallel. Relative magnitudes of the stresses during folding were given by the condition $\sigma_1 > \sigma_3$. It is postulated that σ_2 varied in value as between being equal to σ_1 on one hand, and σ_3 on the other. As a whole, the deformation event responsible for producing the fold is thought to have been characterized by low temperatures (100^{o}-200^{o}), low pressure (2-3 km depth), and low strain rates (10^{-2}-10^{-14} sec^{-1}). Such a combination of variables agrees well with hypotheses for folding style in the Appalachian Valley and Ridge Province.

It is uncertain as to the "exact" timing of lamellae formation in the dynamic history of this fold. Lamellae may have rotated a fair amount into their present orientations after having formed in the very early stages of layer parallel shortening. Alternatively they may have formed virtually "in situ", or have rotated only a very

small amount. The latter explanation assumes that stress refraction has occurred.

Despite these aternatives, it must be emphasized that the general pattern of stresses produced by either option is one of layer parallel compression. Since the fold itself is of very low amplitude and most likely represents a stage of not more that 10% shortening, yet contains deformation lamellae, it can be concluded that lamellae do indeed form in the early stages of fold development when compressive stresses are greatest.

APPENDIX

Nature of Computer (contouring) program

The program is designed to apply a statistical analysis of data using a conventional Gaussian weighting function. This application differs from hand-contouring methods, in that increased refinement of maxima can be obtained. For example, the conventional hand contouring method uses a STEP-FUNCTION as opposed to a WEIGHTED FUNCTION for the data involved. This imposes several limitations, the most drastic of which is that maxima can be artificially flattened, and that artificial maxima or ridges can be produced when two separate clusters are separated from each other by a given amount.

The mathematical theory for the program is derived from Kamb's (1959) statistical analysis for polar and non-polar data (for relevant explanation and equations see p. 210, 211, 212; Robin and Jowett, 1986).

The weighting function applied is;

$$w = \exp (k (\cos\theta - 1))$$

where θ = angle between data point and counting position (as modified from Robin and Jowett, p. 214).

Upon integration, this translates to;

$$E = N (1 - \exp (-2K))/2K$$

where E is the "expected" value of a count for a sample of N data points randomly extracted from a population uniformly distributed over a full sphere.

Varying K is the same as changing α (apical half angle) for a counting circle. In particular, the term exp (-2K) becomes negligible when K > 3 or 4. Under such circumstances an equivalent expression for A (fractional area) is given by;

$$A = 1/K \text{ (for non-polar data)}$$

When K = 100 the parameters of a conventional counting circle are met. These are that A = 0.01 (non-polar data) and $\cos \alpha = 99$ ($R = 8.11^{o}$) (see Robin and Jowett, p. 214).

Standard Deviation

The Gaussian weighting function is a better space averaging tool than the equivalent counting circle (Robin and Jowett, p. 215). Smaller departures from the expected count are therefore more statistically significant. For example, if 400 data points are given, four counts per station are a signficant departure for the conventional counting circle; this contrasts with 3 counts per station taken as significant when the Gaussian weighting function is applied (with K = 100).

Parameters Displayed

All plots were constructed using K = 100. As such, relevant equations, using option 3 of Robin and Jowett, are;

$$E = N/K = N/100$$

$$= 0.07 \ N$$

Captions for Figure 12 and 14 display the K value, E value, and sigma value for each diagram. In all cases, contours are E+2, E+4, E+8 ... E+12 sigma, in accordance with statistically significant (2 sigma) deviations from an expected E (count) value. A typical plot showing data orientations is given in Fig. 24(a). The equivalent contoured data is displayed in Fig. 24(b).

Fig. 24 Example of contouring method.

(a) Data orientations

(b) Contoured data orientations

a

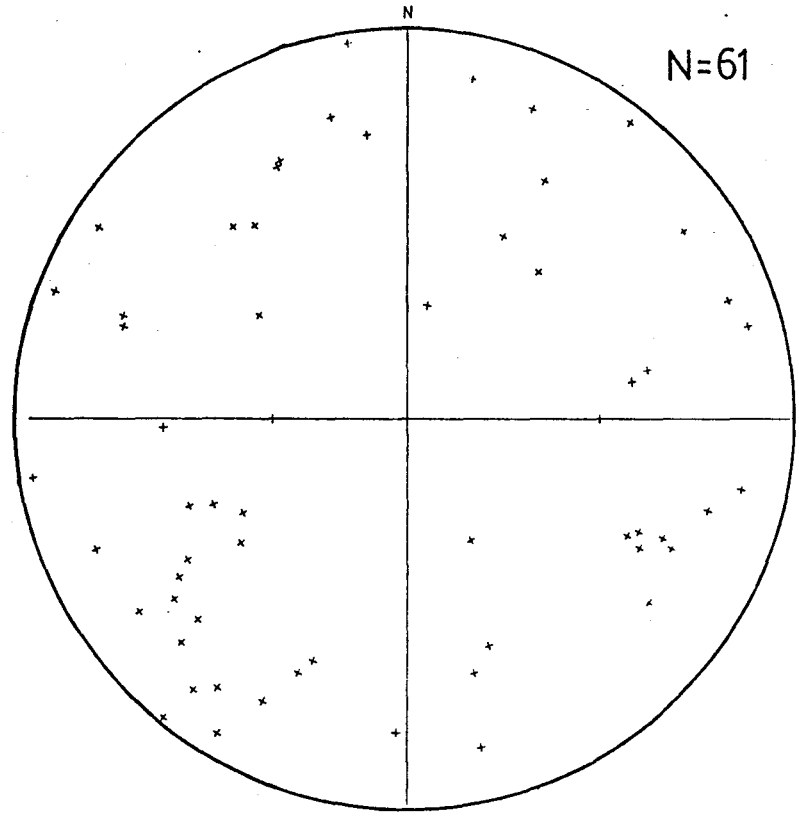

b

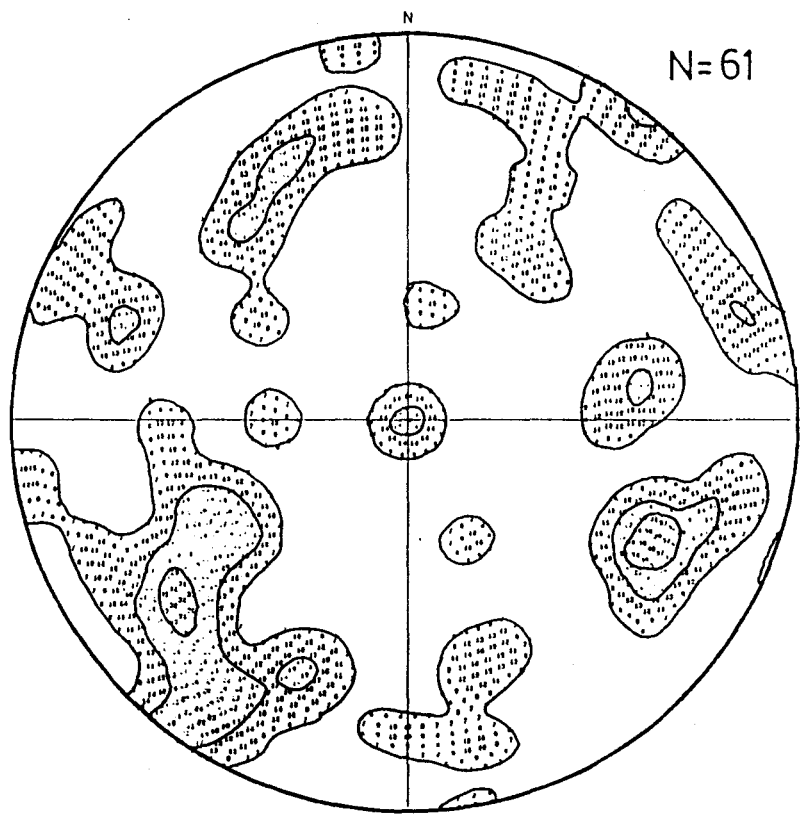

REFERENCES

Ave'Lallemant, H.G.. and Carter, N.L., 1971. Pressure dependence of quartz deformation lamellae orientations: Am. Jour. Sci., v. 270, p. 218-235.

Buhay, W.M., 1985. A study of microstructures in a folded section of the Oriskany Sandstone of central Pennsylvania: B.Sc. Thesis, McMaster University, xii, 99 p.

Carter, N.L., 1976. Steady State Flow of Rocks: Reviews of Geophysics and Space Sciences, v. 14, no. 3, p. 301-353.

Carter, N.L., Christie, J.M., and Griggs, D.T., 1964. Experimental deformation and recrystallization of quartz: Jour. Geology, v. 72, p. 687-733.

Carter, N.L., and Friedman, M., 1965. Dynamic analysis of deformed quartz and calcite from the Dry Creek Ridge Anticline, Montana: Am. Jour. Sci., v. 263, p. 747-785.

Carter, N.L., and Raleigh, C.B., 1969. Principal stress directions from plastic flow in crystals: Geol. Soc. America Bull., v. 80, p. 1231-1264.

Christie, J.M., and Ardell, A.J., 1974. Substructure of deformation lamellae in quartz: Geology, v. 2, p. 405-408.

Christie, J.M, Griggs, D.T., and Carter, N.L., 1964. Experimental evidence of basal slip in quartz: Jour. Geology, v. 72, p. 734-756.

Christie, J.M., and Raleigh, C.B., 1959. The origin of deformation lamellae in quartz: Am. Jour. Sci., v. 257, p. 385-407.

Dietrich, J.H., and Carter, N.L., 1969. Stress-history of folding: Am. Jour. Sci., v. 267, p. 129-151.

Epstein, J.B., and Harris, L.D., 1977. Conodont colour alteration - an index to organic metamorphism: U.S. Geol. Survey Prof. Paper 995, 27 p.

Fairbairn, H.W., 1941. Deformation lamellae in quartz from the Ajibik Formation, Michigan: Geol. Soc. America Bull., v. 52, p. 1265-1278.

Hansen, E., and Borg, I.Y., 1962. The dynamic significance of deformation lamellae in quartz of a calcite-cemented sandstone: Am. Jour. Sci., v. 260, p. 321-336.

Harris, A.G., 1979. Conodont colour alteration, and organo-mineral metamorphic index, and its application to Appalachian Basin geology: The Society of Economic Paleontologists and Mineralogists Special Publication No. 26, p. 3-16.

Heard, H., and Carter, N.L., 1968. Experimentally induced "natural" intragranular flow in quartz and quartzite: Am. Jour. Sci., v. 266, p. 1-42.

McLaren, A.C., Turner, R.G., and Boland, J.N., 1970. Dislocation structure of the deformation lamellae in synthetic quartz; A study by electron and optical microscopy: Contrib. Mineral. Petrol., v. 29, p. 104-115.

Ramsay, J.G., 1967. Folding and Fracturing of Rocks, McGraw Hill, 533 p.

Robin, P.Y.F., and Jowett, E.C., 1986. Computerized density contouring and statistical evaluation of orientation data using counting circles and continuous weighting functions: Tectonophys., v. 121, no. 2-4, p. 207-224.

Scott, H.S., Hansen, E., and Twiss, R.J., 1965. Stress analysis of quartz deformation lamellae in a minor fold: Am. Jour. Sci., v. 263, p. 729-746.

Turner, F.J., 1948. Note on the tectonic significance of deformation lamellae in quartz and calcite: Am. Geophys. Union Trans., v. 29, p. 556-569.

White, S., 1973b. Deformation lamellae in naturally deformed quartz: Nature Phys. Sci., v. 245, p. 26-28.